Tommy Mokkelbost

Synthesis and Characterization of CeO_2 - and $LaNbO_4$ -based Ionic Conductors

Thesis for the degree of philosophiae doctor

Trondheim, September 2006

Norwegian University of
Science and Technology
Faculty of Natural Sciences and Technology
Department of Materials Science and Engineering

NTNU
Innovation and Creativity

NTNU
Norwegian University of Science and Technology

Thesis for the degree of philosophiae doctor

Faculty of Natural Sciences and Technology
Department of Materials Science and Engineering

ISBN 82-471-8134-7 (printed ver.)
ISBN 82-471-8133-9 (electronic ver.)
ISSN 1503-8181
IMT-Report 2006:84 IUK-Thesis 120

Doctoral Theses at NTNU, 2006:181

Printed by Tapir Uttrykk

This thesis has been submitted to

Department of Materials Science and Engineering

Norwegian University of Science and Technology

in partial fulfillment of the requirements for

the academic degree

Philosophiae Doctor

September 2006

PREFACE

First, I would like to express my sincere gratitude to my supervisor Professor Mari-Ann Einarsrud. Your excellent supervision and guidance in addition to your wide knowledge in material science is highly appreciated. I also want to thank you for your encouragement which has been very important for me. I'm also very grateful to my co-supervisor Professor Tor Grande for your enthusiasm and good ideas completing Mari-Ann in an excellent way. Their valuable comments to the draft of this thesis are most appreciated. I'm also grateful for the ideas and comments from Associate Professor Kjell Wiik, Dr. Ingeborg Kaus and Dr. Hilde Lea Lein.

Part of the work presented in this thesis have been carried out by the following co-authors and are highly appreciated:

- Professor Mats Nygren, Dr. Zhe Zhao and Mats Johnsson for operating the spark plasma sintering apparatus.
- MSc. Øystein Andersen and MSc. Ruth Astrid Strøm for developing the wet-chemical route for preparing $LaNbO_4$-based powders.
- Dr. Ingeborg Kaus for performing parts of the solubility studies of SrO in $LaNbO_4$
- Professor Truls Norby and Dr. Reidar Haugsrud, University of Oslo, for electrical conductivity measurements on $LaNbO_4$.
- Professor Randi Holmestad and Dr. Per Erik Vullum for TEM work on $LaNbO_4$.

Financial support from Norwegian University of Science and Technology and the Research Council of Norway, Grant No.1585171431, is appreciated.

I also want to thank the technical personnel at the department, especially Elin Nilsen for guidance to XRD and SEM.

I will thank all my friends and colleagues at "Blokk 2" for making the years pleasant socially, practically and professionally. A special thank to my office-mates Paul Inge Dahl and Johann Mastin for all relevant and irrelevant discussions and making the writing of the thesis more pleasant.

Finally, I want to thank my dear Helene, my daughter Amanda and my family for supporting me through these years, even though the topic is a bit strange for you…Thanks.

TABLE OF CONTENT

SCIENTIFIC PAPERS

APPENDICES

LIST OF ACRONYMS

CGO	$(CeO_2)_{0.8}(GdO_{1.5})_{0.2}$
CSO	$(CeO_2)_{0.8}(SmO_{1.5})_{0.2}$
EDS	Energy Dispersive x-ray Spectroscopy
FE-SEM	Field Emission Scanning Electron Microscopy
G/N	Glycine to Nitrate (ratio)
HP	Hot Pressing
HTXRD	High Temperature X-Ray Diffraction
$p(O_2)$	Partial Pressure of Oxygen
SEM	Scanning Electron Microscopy
SEVNB	Single Edge V-Notch Beam
SOFC	Solid Oxide Fuel Cell
SPS	Spark Plasma Sintering
TEC	Thermal Expansion Coefficient
TEM	Transmission Electron Microscopy
TGA	Thermo Gravimetrical Analysis
WDS	Wave Dispersive x-ray Spectroscopy
XRD	X-Ray Diffraction
YSZ	Yttria-Stabilized Zirconia

1. SUMMARY

Ceramic electrolytes that conduct either oxygen ions or protons at intermediate temperatures are important materials for use in e.g. solid oxide fuel cells, the prime candidate to produce electricity by electrochemical reactions. There are still challenges with respect to the cell performance which have to be solved before solid oxide fuel cells become a commercial success. One of the main topics in this field concerns the enhancement of ionic conductivity at suitable operation temperatures. During the last decade nanocrystalline materials have received considerable attention. Nanocrystalline ionic conductors may have higher ionic conductivity compared to traditional ceramics with grain sizes in the micrometer range.

The aim of this work has been to develop electrolyte ceramic materials with a designed microstructure. CeO_2- and $LaNbO_4$-based materials have been prepared through a complete route, from preparation of powders to densification of ceramics including characterization of selected properties. CeO_2-based materials are oxygen ion conductors and show higher ionic conductivity compared to the more common yttria stabilized zirconia (YSZ), thus a lower operation temperature is possible. $LaNbO_4$-based materials have recently been suggested as a promising proton conductor stable in CO_2/H_2O atmosphere.

In Paper I, powder synthesis of nanocrystalline CeO_2-based powders (CeO_2, $Ce_{0.8}Gd_{0.2}O_{1.9}$ and $Ce_{0.8}Sm_{0.2}O_{1.9}$) using combustion synthesis with glycine as fuel and nitrate as oxidizer is reported. The influence of glycine to nitrate (G/N) ratio on the pure CeO_2-based powders was investigated. The influence of calcination temperature on crystallite size, surface area and carbonate species remaining from combustion reaction was studied, with special attention to powders prepared using a near-stoichiometric G/N-ratio. A G/N-ratio of 0.55 and calcination at 550°C in oxygen flow resulted in high quality powders with a crystallite size of ~10 nm with low degree of agglomeration due to the vigorous combustion. The G/N-ratio influenced the densification behavior of the powders. A G/N-ratio of 0.55 resulted in excellent sintering properties with an onset of sintering at ~600°C and fully dense materials were obtained at ~1300°C.

In Paper II, three different sintering techniques have been used to prepare dense (>95%) CeO_2-based materials from the high-quality powders described in Paper I: Spark plasma sintering, hot pressing and conventional sintering. The three different sintering techniques resulted in different grain sizes, ranging from 160 nm by spark plasma sintering, to 50 μm by

conventional sintering mainly due to difference in sintering temperature and the applied pressure. The materials were reduced after hot pressing and a minor reduction was observed after spark plasma sintering. The materials were easily reoxidized at temperatures above 200°C. The electrical conductivity, measured by van der Pauw method, revealed no clear dependence on grain size, but instead a dependence on the sintering method used. The substituted materials prepared by hot pressing had a lower electrical conductivity and higher activation energy compared to the materials prepared by both conventional and spark plasma sintering. Thus, it is proposed that the reduction of Ce observed during hot pressing might be detrimental for the ionic conductivity even after reoxidation. Hardness and fracture toughness, measured by Vickers indentation, were more influenced by chemical composition than the grain size of the materials. Higher fracture toughness and lower hardness were observed for pure CeO_2 compared to the substituted materials.

A novel route to prepare large quantity of sub-micron $LaNbO_4$-based powders by spray pyrolysis is presented in Paper III. An aqueous solution containing stable La-EDTA complex and Nb-malic acid complex was spray pyrolysed using an in-house spray pyrolysis unit. The pure, non-agglomerated powders had a particle size of ~0.1 μm, narrow particle size distribution and high purity after calcination at 800°C.

The sintering behavior, microstructure, phase content and electrical conductivity of $La_{1-x}A_xNbO_4$ (x = 0, 0.005 and 0.02 and A = Ca, Sr and Ba) prepared by spray pyrolysis is presented in Paper IV. The powders had excellent sintering properties and achieved high density after conventional sintering at 1200°C or as low as 1050°C by hot pressing at 25 MPa. A grain size down to 0.4 μm was achieved by hot pressing. The acceptor doped materials had a more homogenous microstructure due to secondary phases inhibiting grain growth compared to pure $LaNbO_4$. Liquid secondary phase was formed at elevated temperatures in acceptor doped $LaNbO_4$, resulting in tremendous grain growth (~70 μm) and microcracking in $La_{0.98}Ba_{0.02}NbO_4$. The solubility of Sr on La-site in $LaNbO_4$ was determined to 1% at 1500°C, and similar low solubility of CaO and BaO in $LaNbO_4$ was inferred. Protons were found to be the main charge carrier up to 1000°C in wet hydrogen. Higher grain boundary resistivity was observed compared to previous work, possibly due to lower sintering temperature resulting in secondary phases due to lower solubility of AO.

The thermal and mechanical properties of $LaNbO_4$-based materials are presented in Paper V. The materials possessed a ferroelastic to paraelastic phase transition at ~500°C and the linear thermal expansion was significant

lower for the paraelastic compared to the ferroelastic phase. The pure $LaNbO_4$ had a significantly lower hardness compared to acceptor doped (Ca, Sr and Ba) $LaNbO_4$ due to large grain size and microcracking. The fracture toughness of $La_{0.98}Sr_{0.02}NbO_4$, measured by SEVNB method, was 1.7±0.2 $MPa \cdot m^{1/2}$. The ferroelastic properties were confirmed by non-linear stress-strain relationship and remnant strain. The remnant strain decreases with increasing temperature and increasing acceptor doping. The latter was possibly due to secondary phases pinning the ferroelastic domain boundaries.

2. MOTIVATION

During the last 100 years, the energy consumption has dramatically increased especially in the industrial parts of the world due to a more modern lifestyle. The most commonly used sources for energy have been, and still are, fossil fuels which cause environmental pollution. To inhibit problems with environmental pollution there is a large effort in searching for new materials which can be used in new technologies. Fuel cells, which take advantage of the large resources of natural gases, are one of the best candidates to produce electricity with high efficiency by electrochemical reactions combined with low emission of pollutants. There are several different fuel cells under active development: Alkaline fuel cells, polymeric-electrolyte-membrane fuel cells, molten-cabonate fuel cells and solid-oxide fuel cells (SOFCs) [1]. Among these, SOFCs with either oxygen ion or proton conducting electrolytes will be discussed here.

The key feature of SOFCs is its high energy conversion efficiency, since it converts the chemical energy of the fuel directly to electrical energy without the intermediate of thermal energy. A SOFC consists of two porous electrodes separated by a dense ceramic electrolyte. The cells are connected by interconnects to increase the voltage [2]. All these materials must be chemical stable to each other and surrounding atmospheres and have suitable thermal and mechanical properties. Dense electrolytes with high ionic conductivity and low electronic transfer number is necessary [3]. For this purpose, ceramic materials are used. A typical SOFC with oxygen conducting electrolytes could be composed of: $LaMnO_3$-based cathode, yttria-stabilized zirconia (YSZ) electrolyte, Ni-YSZ anode and $LaCrO_3$-based interconnects [3]. A decrease in operation temperature to ~500°C is desirable due to increased life-time for the fuel cell and the possible utilization of metallic interconnects which are inexpensive and possess a high electronic conductivity.

Figure 1 shows a schematic drawing of a high temperature H_2/air fuel cell with an electrolyte of proton conducting Ca-doped lanthanum orthoniobate ($LaNbO_4$), after Norby and Haugsrud [4]. Hydrogen, which is fed at the anode, is oxidized and electrons are liberated. Protons migrate through the electrolyte as illustrated in Figure 1. At the cathode protons, oxygen and electrons from the external circuit form water, an environmentally friendly waste product. In a SOFC with an oxygen ion conducting electrolyte, air is reduced to oxygen ions at the cathode. The oxygen ions migrate through oxygen vacancies in the electrolyte until the fuel (e.g. H_2, CH_4) is oxidized at the anode and water is produced (and CO_2 if hydrocarbons are used). In

both cases electrons are transported through an external circuit from the anode to the cathode and the direct current is utilized in different electrical devices.

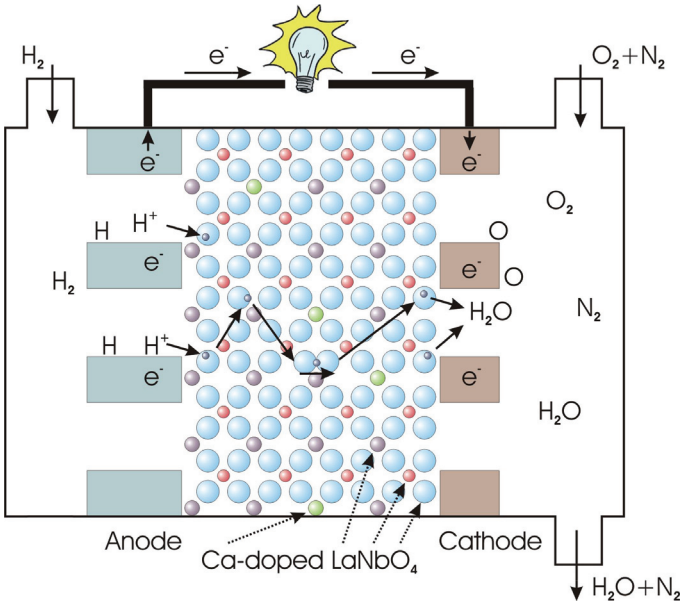

Figure 1 *Schematic solid oxide fuel cell with a proton conducting electrolyte of Ca-doped $LaNbO_4$. H_2 is fed at the anode, oxidized and the protons are transported through the electrolyte to the cathode where water is formed in combination with O_2. Arrows inside the electrolyte point out hydrogen pathways [4].*

In a SOFC composed of oxygen ion conducting electrolyte the water vapor produced on the fuel side will dilute the fuel and therefore a continuous fuel recycling is required. High temperature SOFCs using proton conducting electrolytes have no dilution of the fuel since water vapor is not produced on the fuel side. Thus, the advantage using a proton conducting electrolyte results in a fuller utilization of the fuel [4].

Even though the research on SOFCs has been going on for several decades there are still challenges to be overcome. A lower operation temperature demanding higher ionic conductivity, new materials with high proton conductivity and stability in CO_2 and H_2O atmosphere and that the cost of electricity per kWh is too high to compete with the energy technology of today [1] are examples of topics that need more attention. Though, more research and development of suitable ceramic oxide materials with optimized properties are necessary.

2.1. Aim of work

The overall aim of the work presented in this thesis has been to develop complete preparation routes to selected oxygen and proton conducting electrolyte materials with a designed homogenous microstructure. The preparation routes should include a complete study from powder synthesis through final densification. Further, the prepared materials should be carefully characterized with the respect to selected electrical and mechanical properties to reveal microstructure-property relations.

Both traditional and new candidates for ceramic electrolytes have been studied. Among the traditional oxygen ion conducting materials cerium oxide (ceria, CeO_2) based materials have received considerable interest due to their higher ionic conductivity compared to the more common electrolyte YSZ. But still there are challenges to overcome for CeO_2-based materials before the materials can be fully utilized. The ionic conductivity must be further improved to achieve lower operation temperatures and the mechanical properties must be optimized.

The state-of-the-art proton conductors for application in SOFCs, Ba- or Sr-based cerates or zirconates, show low stability in CO_2 and H_2O containing atmospheres. Recently, acceptor doped (Ca, Sr) $LaNbO_4$ which are stable in operating atmospheres have been reported as candidates for proton conducting electrolytes and these materials were hence, chosen for the present studies.

To optimize the electrical and mechanical properties of any material care must be taken in both powder synthesis and densification. Hence, this work reports a complete study from powder synthesis to densification with characterization of selected properties for both CeO_2- and $LaNbO_4$-based materials. For CeO_2-based materials the aim of work was to prepare bulk materials with different designed nano- and microstructures. For this purpose an inexpensive combustion synthesis route using glycine as fuel and complexing agent and nitrate as oxidizer was chosen to prepare high quality, non-agglomerated nanocrystalline powders. To study the effect of microstructure, and especially grain size, the powders were sintered using three different techniques. Both mechanical and electrical properties are thought to depend on grain size, especially by decreasing the grain size to nanometer regime. Thus, these properties were investigated.

To prepare $LaNbO_4$-based powders a synthesis route combining large quantity and high quality was desirable and spray pyrolysis was chosen. A route to prepare aqueous solution to prepare $LaNbO_4$ by spray pyrolysis was

necessary to be established. Optimal densification routes are not known for these materials and therefore extensive sintering studies using conventional sintering and hot pressing were performed. To optimize the proton conductivity of $LaNbO_4$-based materials the solubility of the acceptors CaO, SrO and BaO in $LaNbO_4$ should be determined. Hence, the sintering studies, solubility and proton conductivity measurements were conducted. The mechanical and thermal properties are also scarcely reported in literature and were therefore studied. To determine the influence on acceptor doping to mechanical properties, stress-strain behavior, hardness and fracture toughness were studied for different materials. Due to the ferroelastic behavior of $LaNbO_4$, the contribution of ferroelasticity to fracture toughness was discussed.

3. INTRODUCTION

3.1. Crystal structure

3.1.1. CeO_2

CeO_2 crystallizes in the cubic fluorite structure (CaF_2 structure) which is illustrated in Figure 2. Each Ce atom is surrounded by eight equivalent nearest neighbor O atoms. The O atoms are further surrounded by a tetrahedron of four equivalent Ce atoms [5]. The fluorite structure is relatively open with large (½, ½, ½) octahedral holes and shows large tolerance for atomic disorder due to e.g. substitution, reduction or oxidation.

CeO_2 is pale yellow due to Ce(IV) - O(-II) charge transfer. CeO_2 can be considerably reduced without phase change [6]. The ordering of vacancies in CeO_{2-x} results in a number of phases with $CeO_{1.714}$ as the most reduced phase within the "fluorite-like" region [7]. During reduction to CeO_{2-x}, a color change to blue with minor reduction or to almost black at major reduction occurs [6].

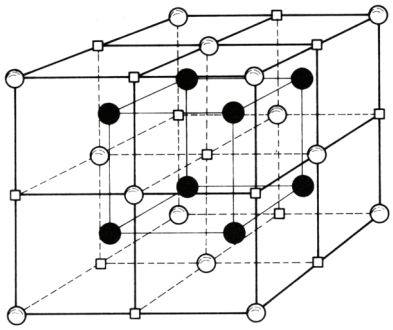

Figure 2 The fluorite structure after Matzke [5]. ○ = cation (e.g. Ce), ● = anion (e.g. O) and □ = interstitial positions.

3.1.2. $LaNbO_4$

$LaNbO_4$ crystallizes in a monoclinic (m) phase [8] isostructural with fergusonite below and in a tetragonal (t) phase [9] isostructural with scheelite above a phase transition temperature at ~500°C [10-13]. Figure 3 shows the low temperature monoclinic phase of $LaNbO_4$. In both polymorphs, the La^{3+} has a coordination number of 8 and Nb^{5+} a

coordination number of 4 [9]. The monoclinic structure can be regarded as a distorted tetragonal structure. At the transition temperature the lattice parameters $a_m \rightarrow c_t$, $c_m \rightarrow a_t$ and $b_m \rightarrow c_t$. The angle between a_m and c_m, β, decreases continuously from ~94° to 90° approaching the transition temperature.

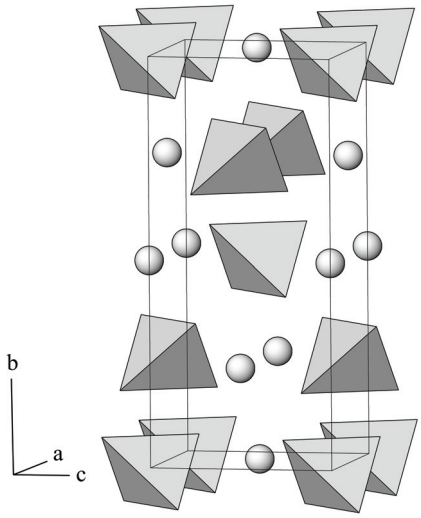

Figure 3 Low temperature, monoclinic polymorph of $LaNbO_4$ based on crystallographic data from Tsunekawa et al. [8]. Tetrahedra are NbO_4 and spheres depict La ions.

3.2. Ionic conductors

Materials that conduct ions, known as solid electrolytes, are today commonly used in many different applications. The ionic migration proceeds via defects, either vacancies or interstitials, and the structure should therefore exhibit a high level of disorder. In addition, the ionic conduction can be accompanied by electronic conduction. Depending on the desired application, the material could be tailored with acquired properties. The focus here will be solid electrolytes of CeO_2- and $LaNbO_4$-based materials where either oxygen ions or protons, respectively, are the conductive ions.

3.2.1. CeO_2-based oxygen ion conductors

The electrical conductivity of different ceramic electrolytes is shown in Figure 4 [14]. Bi_2O_3-based oxides exhibit the highest electrical conductivity, but these materials are not suitable for applications in reducing atmospheres since they are unstable and are easily reduced [15]. The most studied electrolytes are materials with the fluorite structure MO_2 (M = Zr, Ce and Hf) with solid solution of $M'O_x$ (M′ = Ca, Sc, Y or rare earth elements) and among these, YSZ has been most studied [3]. CeO_2-based electrolytes [15] have a higher ionic conductivity than the more commonly applied YSZ electrolytes, as shown in Figure 4. A review on properties of CeO_2-based materials is given in the following.

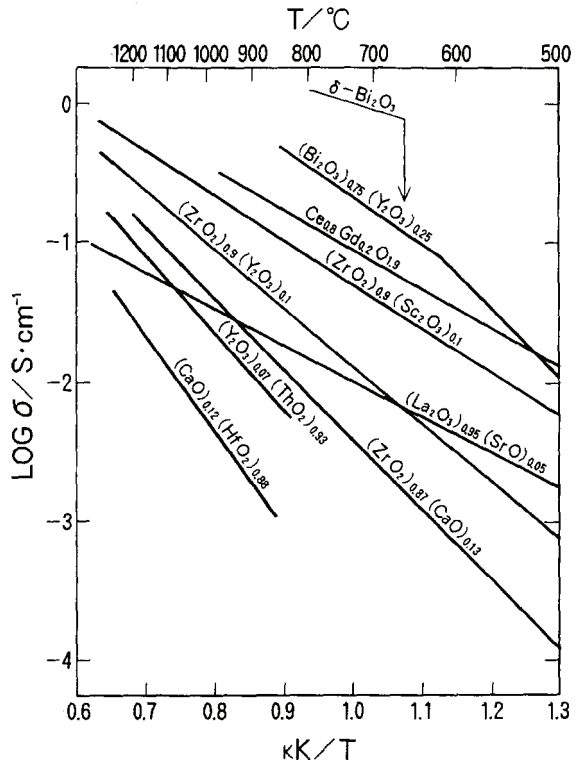

Figure 4: Electrical conductivity in different ceramic electrolytes according to Steele [14].

Electrical conductivity in pure CeO_{2-x}

As mentioned earlier, pure CeO_2 can be considerable reduced without phase changes. The reduction of Ce^{4+} to Ce^{3+} can be described as shown in equation (1):

$$2Ce_{Ce} + O_O = 2Ce'_{Ce} + V_O^{\bullet\bullet} + \frac{1}{2}O_2(g) \qquad (1)$$

Figure 5 shows log x as function of log $p(O_2)$ for CeO_{2-x} at different temperatures after Panlener et al. [16]. The degree of reduction is dependent on temperature and partial pressure of oxygen, $p(O_2)$.

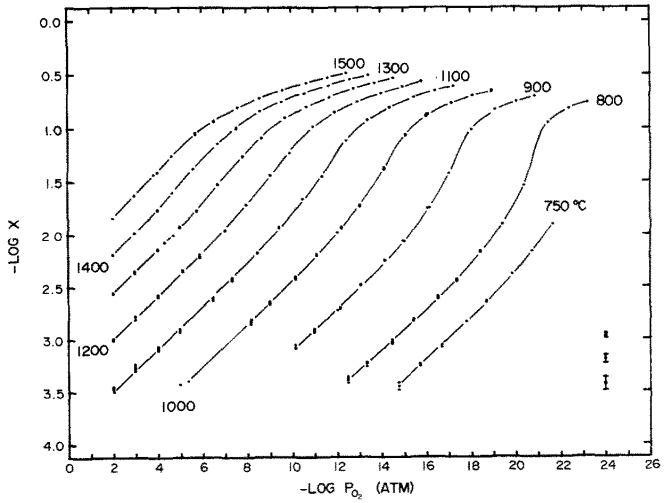

Figure 5 Isothermal log x as function of log $p(O_2)$ for CeO_{2-x} at different temperatures after Panlener et al. [16].

The reduction renders pure CeO_{2-x} a mainly electronic conductor. The n-type conductivity takes place by small polaron transport [17], where charge carriers migrates by thermally activated hopping. Figure 6 shows the conductivity of CeO_y as function of y at 1000°C and corresponding electron hopping energy, E_H, by Tuller and Nowick [17]. The conductivity increased from CeO_2 to $CeO_{1.95}$ stoichiometry from where the conductivity is independent of non-stoichiometry. The corresponding activation energy increased with non-stoichiometry.

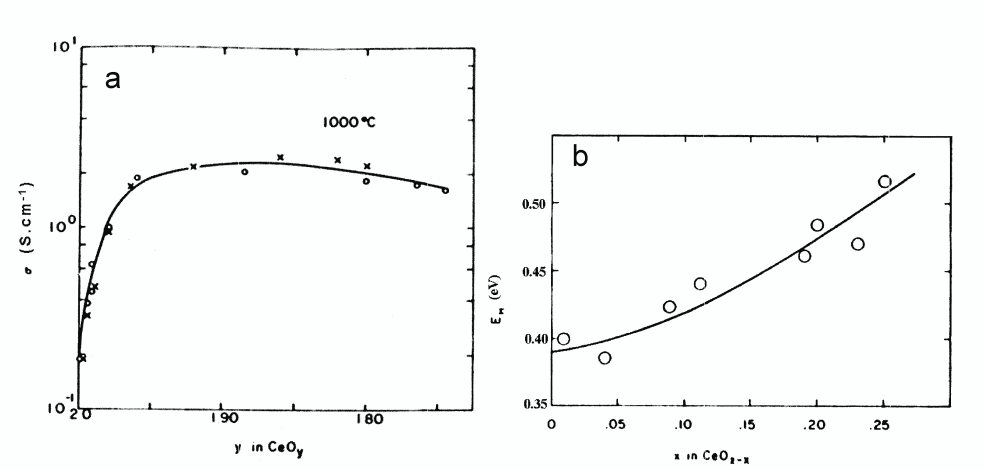

Figure 6 Conductivity at 1000°C as function of y in CeO_y (a) and corresponding electron hopping energy (b). O *from [17] and* X *from [18].*

Effect of substitution on electrical conductivity of CeO_2

Introduction of lower valent cations on Ce^{4+} site results in oxygen vacancies. The dissolution of e.g. Gd_2O_3 into CeO_2 lattice can be written as:

$$Gd_2O_3 = 2Gd'_{Ce} + V_O^{\cdot\cdot} + 3O_O \tag{2}$$

Oxygen ions are transported through oxygen vacancies, thus the ionic conductivity is dependent on the vacancy concentration. A maximum in conductivity is observed in the range of 10-20 mol% substitution due to formation of defect pairs [19], as shown in equation (3).

$$Gd'_{Ce} + V_O^{\cdot\cdot} \rightarrow \left\{Gd'_{Ce}V_O^{\cdot\cdot}\right\} \tag{3}$$

The total conductivity (σ), is dependent of the number of charge carriers (n), the charge carried by each carrier (q) and the mobility of the carriers (μ) and can be expressed by equation (4):

$$\sigma = nq\mu \tag{4}$$

The total conductivity is dependent on temperature (T) which can be expressed by equation (5)

$$\sigma T = A\exp(-E_a / kT) \tag{5}$$

where A is constant, E_a is the activation energy and k the Boltzmann constant.

In addition to the amount of substitution, the type of substitute also influences the ionic conductivity. Figure 7 summarizes the ionic conductivity versus the radii of substituted cations in $(CeO_2)_{0.8}(LnO_{1.5})_{0.2}$. As seen from Figure 7, Sm- and Gd-substituted CeO_2 have the highest ionic conductivity among the CeO_2-based electrolytes [20]. Arai and co-workers [20, 21] suggested $Ce_{0.8}Gd_{0.2}O_{1.95}$ as the best candidate for electrolytes due to higher electrical conductivity and less reducibility than other rare-earth oxide substituted CeO_2 materials. Steele [22] reviewed the thermodynamic and electrical data and selected $Ce_{0.9}Gd_{0.1}O_{1.95}$ as the most appropriate electrolyte for intermediate temperature (IT)-SOFC operating at 500°C. $Ce_{0.9}Gd_{0.1}O_{1.95}$ shows higher conductivity compared to materials with Sm^{3+} or Y^{3+} and lower reducibility compared to $Ce_{0.8}Gd_{0.2}O_{1.9}$. The higher conductivity for $Ce_{0.9}Gd_{0.1}O_{1.95}$ is not in agreement with Figure 7, but could be due to difference in e.g. activation energy or different level of substitution.

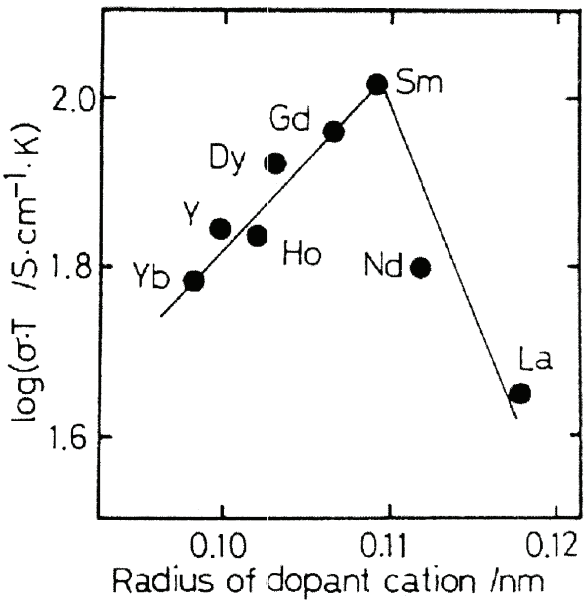

Figure 7 Dependence of the radii of substituted cation on ionic conductivity at 800°C for $(CeO_2)_{0.8}(LnO_{1.5})_{0.2}$ [20].

Figure 8 shows the O/M-ratio, where M = (Gd or Sm) + Ce, versus log $p(O_2)$ at different temperatures for different compositions of Sm- and Gd-substituted CeO_2 summarized by Kobayashi et al. [23]. As seen from Figure 8 the degree of reduction is dependent on temperature, $p(O_2)$ and to some degree composition. Both $Ce_{0.9}Sm_{0.1}O_{1.95}$ and $Ce_{0.9}Gd_{0.1}O_{1.95}$ are stable at $p(O_2) > 10^{-15}$ atm at 700°C. Reduction occurs at higher $p(O_2)$ when higher substitution levels are used and/or the temperature is increased [23-25]. At 700°C substituted CeO_2 is reduced at higher $p(O_2)$ compared to pure CeO_2, but at higher temperatures pure CeO_2 is easier reduced [26].

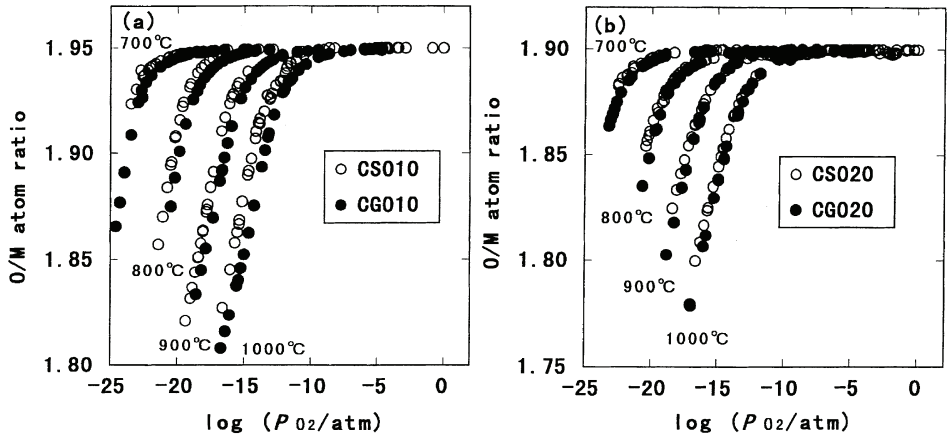

Figure 8 O/M-ratio, where M=(Gd or Sm) + Ce, as function of log $p(O_2)$ at different temperatures [23]. $Ce_{0.9}Gd_{0.1}O_{1.95-x}$ (CGO10) and $Ce_{0.8}Gd_{0.2}O_{1.9-x}$(CGO20) are taken from Wang et al., ref [24] and [25] respectively.

Another challenge is the enhanced electronic conduction in reduced CeO_2-based materials which has to be suppressed. With a thin, dense layer of e.g. YSZ [20, 27, 28] it is possible to suppress the reduction at the fuel side. Inoue et al. [27] demonstrated a higher open circuit by coating $(CeO_2)_{0.8}(SmO_{1.5})_{0.2}$ with YSZ on the fuel side compared to $(CeO_2)_{0.8}(SmO_{1.5})_{0.2}$ without coating. The coated electrolyte also showed higher power density compared to YSZ electrolyte. But even so, different thermal expansion coefficients cause challenges regarding the mechanical properties of the system. Interaction between YSZ and $Ce_{0.90}Gd_{0.10}O_{1.95}$, which decreases the ionic conductivity, only occurs above 1000°C, so for IT-SOFC this is not an issue [29].

Among the divalent cations for substitution, calcium has been most studied, but calcium is not accepted well in the fluorite lattice as it seem to be expelled upon repeated oxidation/reduction cycling or due to long term exposure to high temperature [7].

Effect of microstructure on conductivity of CeO_2

A topic that has attracted great interest during recent years is the possibility to increase the ionic conductivity of polycrystalline oxide conductors by decreasing the grain size into the nanometer range [30]. Two important factors for enhanced ionic conductivity are high defect densities and high defect mobilities. As grain boundaries intrinsically appear to possess these characteristics, enhanced ionic conductivity might be achieved by reducing the grain size and thereby introducing a larger amount of grain boundaries. Any extraneous phases, e.g. SiO_2, or substituent segregation will normally migrate to the grain boundaries making them less conductive than the bulk [31-33]. However, with decreased grain size the impurities might distribute over a higher grain boundary population which again will cause an increase in grain boundary conductivity. An additional factor determining the ionic conduction at grain boundaries is related to the effect of space charge regions in the grains adjacent to the grain boundaries introduced by Maier [34]. If the bulk defect with high mobility, e.g. oxygen vacancies, is accumulated in the space charge region, the grain boundary conductivity should increase. On the other hand, oxygen vacancy depletion resulting from space charge in the vicinity of the grain boundaries or other problems like imperfect alignment between grains might increase the grain boundary resistivity and hence the grain boundary conductivity will decrease with decreasing grain size. Depending on which effect is most dominant, the grain boundary conductivity and hence the ionic conductivity of the material may decrease or increase with decreasing grain size.

Suzuki et al. prepared thin films of CeO_2 which showed an increase in total conductivity by decreased grain size [35], also compared to microcrystalline materials. This increase was explained by an increase in the defect concentration with 3 orders of magnitude from 50 to 10 nm due to a lower enthalpy of oxygen vacancy formation. Chiang et al. [36, 37] showed enhanced electronic conductivity in nanocrystalline bulk materials in agreement with the results of Suzuki [35]. The results demonstrated that stoichiometry can be controlled by microstructure. Tschöpe et al. [38] observed a change in the sign of the Seebeck coefficient as function of grain size in 500 ppm Gd-doped CeO_2, due to transition from ionic to electronic conductivity which is in agreement with Chiang [36, 37]. Tsunekawa et al.

[39] observed an increase in lattice parameters of CeO_2 by decreased particle size below 10 nm due to the conversion of Ce^{4+} to Ce^{3+} ions at the surface. A particle size of 2.6 nm resulted in 74% Ce_2O_3 and 26% CeO_2 according to Vegards law which is in agreement with the ratios of cerium ions at the surface, 75% for this particle size. Similar results have been reported by others [40] and are in agreement with the observed increase in electronic conductivity.

Ionic conduction in nanocrystalline bulk $Ce_{0.74}Gd_{0.26}O_{1.87}$ was not affected by grain size [36]. This is also in agreement with the work of Kosacki et al. [41] who found an increase in defect concentration in CeO_2 thin films, but not in ZrO_2:16%Y thin films. Even so, an enhancement of about two orders of magnitude in the ionic conductivity, at 600°C, for nanocrystalline YSZ was observed due to lower activation energy [42]. For nanocrystalline $Ce_{0.8}Gd_{0.2}O_{1.9}$ films the ionic conductivity increased with decreasing activation energy as the grain size decreased [43]. Even so, the ionic conductivity was 4 times lower than that for microcrystalline specimens. But lightly doped CeO_2 thin films showed electronic conduction when grain size was reduced to the nanometer range.

The grain boundary and grain interior conductivity in microcrystalline $Ce_{0.8}Gd_{0.2}O_{1.9}$ versus grain size (0.7 - 17 μm) has been studied [44]. Above 3 μm the grain boundary conductivity increased while grain interior conductivity was almost constant. Zhou et al. [45] studied the grain boundary conductivity in $Ce_{0.9}Gd_{0.1}O_{1.95}$ with different grain sizes (0.15 - 1.1 μm) and found a higher grain-boundary resistance in samples with the smallest grains, but this effect was eliminated at T>600°C. The grain conductivity was independent on grain size. A continuous decrease in electrical conductivity in $Ce_{0.8}Dy_{0.2}O_{1.9}$ down to a grain size of 0.24 μm and a sudden increase in electrical conductivity by further decrease in grain size was observed by Wang et al. [46]. This was explained by either less continuous blocking layers and/or lower segregation of solutes due to smaller grains. Decreased sintering temperature which resulted in smaller grains, but not dense materials, resulted in higher grain boundary conductivity due to lower impurity concentration at the grain boundaries [31]. But even in SiO_2 free samples the grain boundary conductivity was 2-7 orders of magnitude lower than the bulk conductivity in both pure and yttria-substituted CeO_2, possibly due to oxygen vacancy depletion at the space charge layers [47].

Mori et al. [48] observed large microdomains (10 nm) in the lattice of both Sm- and La-substituted CeO_2, which inhibited the oxide ion conduction through the lattice, resulting in lower electrical conductivity. Substituting

Sm or La together with alkaline earth into CeO_2 resulted in smaller microdomains (1-3 nm) increasing the lattice conductivity. An increase in conductivity by co-doping CeO_2 with Sm and Gd was also observed by Wang et al. [49]. Both the size and morphology of the powder and densification method was found to influence the size of microdomains [50, 51]. By a combination of conventional sintering and spark plasma sintering a further increase in ionic conductivity was observed due to smaller microdomains [51].

The optimal amount of substitution is not established and might also be dependent on impurities. A maximum in grain boundary conductivity in $Ce_{1-x}Gd_xO_{2-\delta}$ was found at $x = 0.15$ in samples with 30 ppm SiO_2 and at $x = 0.20$ in samples with 200 ppm SiO_2. The difference was attributed to reactions between SiO_2 and Gd_2O_3 in the impure materials, reducing the amount of SiO_2 at the grain boundaries. The increase in SiO_2 also reduced the grain boundary conductivity. With increased substitution the grain boundary resistance became vanishing small compared to grain interior conductivity [52, 53]. Zhang et al. [54] systematically studied the ionic conductivity in $Ce_{1-x}Gd_xO_{2-\delta}$ and observed a maximum grain boundary conductivity at $0.1 \leq x \leq 0.2$ and rapid decrease in conductivity when $x > 0.2$. The latter can be attributed to microdomains blocking the mobility of oxygen ions or precipitated secondary phase. Zha et al. [55] observed a maximum in conductivity at $x = 0.15$.

Zhang et al. demonstrated that adding small amounts of Fe_2O_3 to $Ce_{0.9}Gd_{0.1}O_{2-\delta}$ [56] and $Ce_{0.8}Gd_{0.2}O_{2-\delta}$ [57] had a scavenging effect on SiO_2 impurities and a higher grain boundary conductivity was observed. The scavenging effect could be attributed to: 1) Trapping of SiO_2 at the Fe_2O_3 interfaces and/or 2) modification of viscosity and wetting nature of SiO_2 layers due to dissolution of Fe_2O_3. Other oxides added as sintering aids, e.g. Al_2O_3 [58], MnO [59] and CoO [60], have shown a detrimental effect in the conductivities, especially on the grain boundary conductivity.

Both thin films and bulk materials of nanocrystalline pure CeO_2 materials are easier reduced compared to microcrystalline CeO_2 due to lower enthalpy of oxygen vacancy formation which results in an increased electronic conductivity. For substituted CeO_2, an increase in ionic conductivity by reducing the grain size to nanometer region has not been demonstrated. The ionic conductivity have been increased by reducing the size of the microdomains, diluting the impurity concentration by reduced grain size and adding Fe_2O_3 which has a scavenging effect on SiO_2 impurities.

3.2.2. Proton conductors

Solid-state proton conductors can be divided into three classes dependent on temperature and materials as follows [61]: 1) Water-containing systems where proton exchange membranes (PEM) based on polymers are used at low temperatures, e.g. Nafion. 2) Low temperature inorganic proton conductors, such as $CsHSO_4$. 3) High temperature proton conductors like acceptor doped perovskites, e.g. $SrCeO_3$ and $BaCeO_3$. The latter class of proton conductors will be presented further below.

In 1981, Iwahara and co-workers [62] discovered relative high proton conductivity in acceptor doped $SrCeO_3$ at high temperatures in the presence of water vapor or hydrogen. This discovery initiated extensive research on proton conducting high temperature ceramics.

Potential applications of high temperature proton conductors are fuel cells, steam electrolysis, hydrogen pumps, humidifiers, dehydrogenation and hydrogenation of hydrocarbons, sensors [63] and electrochromic devices [64].

The proton conductivities of various oxides, calculated from data from Norby and Larring [63] and Haugsrud and Norby [65], are shown in Figure 9. Among the perovskites $BaCeO_3$- and $BaZrO_3$-based materials show the highest proton conductivity with a maximum in proton conductivity, about 10^{-2} S/cm, at ~800°C. The observed maximum in proton conductivity is a typical behavior observed for high temperature proton conductors due to less dissolution of protons at high temperatures [66]. At high temperature these materials become oxygen ion conductors. The drawback of these materials is low stability in reducing atmosphere. They can decompose, react to carbonates or form alkaline earth hydroxides in CO_2 or H_2O atmospheres [67], which excludes hydrocarbons as fuels.

In addition to the perovskites of ABO_3, perovskites of more complex structures, e.g. $A_2(B'B'')O_6$ and $A_3(B'B'')O_9$ have been studied by Nowick et al. [68, 69]. Among these $Ba_3(Ca_{1.18}Nb_{1.82})O_{9-\delta}$ (BCN-18) exhibited the highest conductivity, $\sim 2 \cdot 10^{-3}$ S/cm. Proton conduction in acceptor doped rare-earth sesquioxides, which are stable in CO_2/H_2O atmosphere, has also been demonstrated and a conductivity of $7 \cdot 10^{-4}$ S/cm was observed in Ca-doped Gd_2O_3 at 900°C [70]. Also shown in Figure 9 are Sr-substituted $LaPO_4$ with a proton conductivity of $3 \cdot 10^{-4}$ S/cm at 800°C [71]. Among the phosphates, Sr-doped LaP_3O_9, shows the highest proton conductivity, $3 \cdot 10^{-4}$ S/cm at 700°C, but this material has a limited stability at higher temperatures [72].

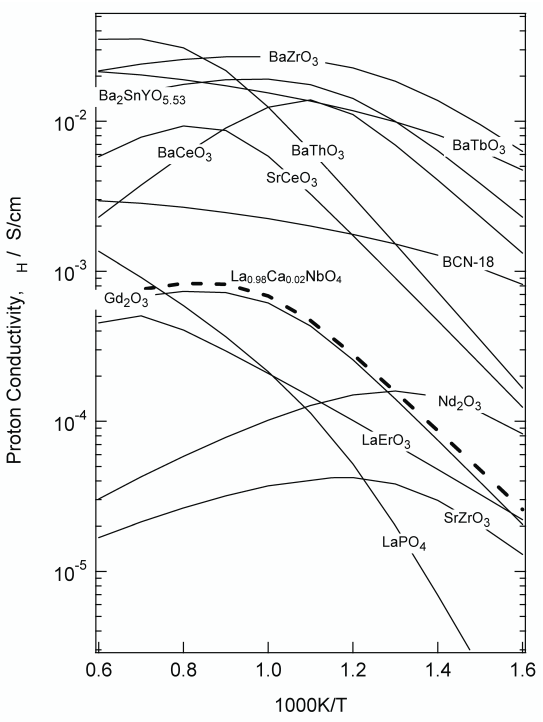

Figure 9 Proton conductivities of various oxides [73] calculated from data from Refs. [63]and [65].Type of dopant is not indicated (except for $LaNbO_4$), but could be found in Ref. [63].

Recently, a new type of proton conducting materials based on rare-earth orthoniobates ($RENbO_4$) has been proposed by Haugsrud and Norby [65, 66, 74]. Among these, acceptor doped $LaNbO_4$ have the highest proton conductivity, ~10^{-3} S/cm. The total and partial protonic conductivity of 1% Ca doped $RENbO_4$ is shown in Figure 10. Acceptor doped $LaNbO_4$ has the highest proton conductivity among $RENbO_4$ due to a more favorable hydration enthalpy when the size of the rare earth cation decreases. The protons are the major charge carrier up to ~950°C, dependent on composition, where oxygen ion conductivity starts to contribute. The conductivity in the tetragonal phase is less temperature dependent due to more favorable hydration enthalpy compared to the monoclinic low temperature phase. Thus, $RETaO_4$, which exhibit a higher phase transition temperature, will have lower proton conductivity compared to the $RENbO_4$.

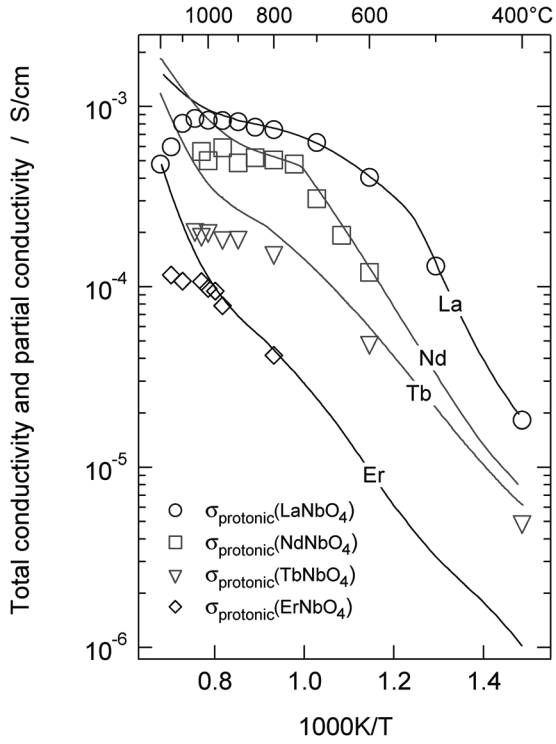

Figure 10 Total (solid line) and partial proton (symbols) conductivities versus temperature for 1% Ca-doped $RENbO_4$ (RE = La, Nd, Tb, Er) in wet H_2 atmosphere [65].

Still, the proton conductivity of $LaNbO_4$-based materials is lower compared to the state-of-the-art proton conductors like $BaCeO_3$, but they have the advantages of being stable in CO_2 and H_2O containing atmospheres.

To ensure high proton conductivity in high temperature proton conductors, oxygen vacancies are proposed to be necessary. In perovskites as e.g. $SrCeO_3$ vacancies are introduced in the lattice by substituting Ce with a lower valent cation, e.g. Yb^{3+}. Protonic defects [67] are formed when water from the wet gas phase dissociates into one proton and one hydroxide ion, where the hydroxide ion fills an oxygen vacancy. Due to the small ionic radius of the proton, the protons cannot occupy a vacancy or a normal interstitial site in an oxide. Thus, the protons form hydroxide with a lattice oxygen as described by equation (6):

$$H_2O + V_O^{\bullet\bullet} + O_O = 2OH_O^{\bullet} \qquad (6)$$

If oxygen is present, the dissolution of oxygen to produce holes will compensate for the available oxygen ion vacancies [75]

$$2V_O^{\bullet\bullet} + O_2 = 2O_O + 4h^{\bullet} \quad (7)$$

From the two equations above, protonic, oxygen ion and p-type electronic conductivity is possible depending on water vapor pressure, partial pressure of oxygen and hydrogen, substitution and temperature. Proton transport can occur in two ways. The transport of protons among relatively stationary host anions like in high temperature proton conductors is termed Grotthuss or free-proton mechanism. Transport of protons by other species, e.g. OH^-, H_2O, H_3O^+ is termed vehicle mechanism [61].

3.3. Synthesis of bulk materials

3.3.1. Powder synthesis

To prepare ceramic materials with a homogenous and controlled microstructure, low impurity content and suitable properties the powder synthesis is always crucial. Here, different synthesis routes to prepare nanocrystalline CeO_2-based powders and $LaNbO_4$-based powders are reviewed from the literature.

To prepare nanostructured ceramic materials the starting powder must be of high quality which implies phase pure nanosized powder with narrow particle size distribution, no, or usually minimal, impurities and low degree of agglomeration. A non-agglomerated powder with narrow particle size is important to inhibit grain growth and to achieve a homogenous grain size distribution with small grains. Impurities might result in secondary phases, which could be favorable to inhibit grain growth but could e.g. also cause liquid phase sintering giving exaggerated grain growth. Impurities forming gaseous spices might cause porosity deteriorating the mechanical and electrical properties.

CeO_2-based powders

Several different synthesis routes have been reported to prepare nanosized CeO_2-based powders and selected routes are described here. Combustion synthesis is a low cost synthesis route to prepare nanocrystalline powders.

Reviews of combustion synthesis are made by Patil et al. [76, 77]. Both solid state and solution combustion are common, but only solution combustion have been reported for CeO_2-based materials. Different fuels and complexing agents have been used, e.g. glycine [78-83], citric acid [84], oxalyldihydrazine [85, 86], ethylene glycol [87] and carbohydrazide [86]. Glycine-nitrate method is a self-sustaining combustion process that is rapid and yields the final oxide product almost directly. Appropriate ratios of metal nitrates are dissolved with e.g. glycine which works as both a complexing agent and fuel. The flame temperature, product oxidation state and crystallite size can be controlled by adjusting the glycine to nitrate (fuel to oxidant) ratio [80, 81, 83, 88]. Comparing glycine-nitrate to amorphous citrate process for synthesis of lanthanum strontium chromite (LSC), a more homogenous composition was obtained by the glycine-nitrate route [88]. Park et al. [89] produced $(CeO_2)_{0.9}(Gd_2O_3)_{0.1}$ by glycine-nitrate process and demonstrated better sintering behavior compared to commercial powder. Duran et al. [90] prepared CeO_2 with citric acid, polyvinylalcohol and polyethylene glycol and studied the influence of these complexing agents on the sintering behavior. Sintering temperatures of 1250°C, 1380°C and >1650°C, respectively, was necessary to obtain 98% dense materials mainly due to differences in pore-size distributions in the green compacts. Due to the vigorous combustion of CeO_2-based powders the gaseous species formed will partly inhibit agglomeration and form weak agglomerates which are easily broken down during e.g. ball milling [78, 80, 89].

Another well-studied route to prepare CeO_2-based powders is direct precipitation method. Using e.g. hexamethylenetetramine (HMT) and nitrates of the desired cations is perhaps the most common route to prepare nanocrystalline CeO_2-based powders [91-94]. By this precipitation method, Chen et al. [92] demonstrated that the densification behavior was independent of calcination temperature even tough the crystallite size increased. Weakly agglomerated, nanosized CeO_2 powders have been prepared by a two stage precipitation-hydrothermal process [93, 95]. Hydrogen peroxide (H_2O_2) added to $Ce(NO_3)_3$ at 5°C slowly oxidized Ce^{3+} to Ce^{4+} and initiated homogenous precipitation of spherical agglomerates which were disrupted by addition of NH_4OH, leaving a weakly agglomerated powder after hydrothermal treatment at 180°C. Generally, calcined powders are agglomerated, but this could be inhibited using an anion surfactant like sodium hexametaphosphate [96]. Precipitation of CeO_2 powder using hydrazine monohydrate [97] and oxalate precipitation of $Ce_{0.8}RE_{0.2}O_{1.9}$ (RE = Yb, Y, Gd, Sm, Nd and La) [98] have also been reported.

Carbonate co-precipitation is also a suitable route to prepare different CeO_2-based powders. Carbonates as precursors are nongelatinous and show much

weaker agglomeration after drying compared to hydroxides [99]. Li et al. [99] used urea and ammonium bicarbonate (AHC) which resulted in different particle morphologies. Weakly agglomerated nanoparticles were formed from AHC method whereas monodispersed submicrometer-sized spheres with sub-structures were formed from the urea method, resulting in different sintering properties. Powder from AHC method was dense after 1050°C while 1400°C was necessary using the urea method. The influence of size of substitute on agglomeration by precipitation using ammonium carbonate was studied by the same group [100]. Large cations (La, Nb Sm) were mainly composed of secondary agglomerates of fibrous primary particles, while the smaller cations (Gd, Dy, Y, Ho, Er and Yb) resulted in powders of discrete primary spherical particles. Other CeO_2-based powders have been prepared by similar route using ammonium carbonate [100-103].

CeO_2 has also been synthesized by mechanochemical reaction between $CeCl_3$ and NaOH in dilute NaCl resulting in particle size in the range of 10 to 500 nm depending on calcination temperature [104]. Mechano-chemical reaction of $Ce_2(CO_3)_3$ with NaOH resulted in agglomerated nanocrystalline CeO_2 [105]. The same procedure using CaO, instead of NaOH, resulted in a crystallite size of ~19 nm [106]. Addition of NaCl decreased the degree of agglomeration during calcination [107].

To prepare nanosized powders in large quantities, spray pyrolysis is a good option. Gd-substituted CeO_2 particles have been prepared by this method [108]. The morphology and particle size was dependent on the type of solvent. Particles prepared from a solution containing ethylene glycol had loosely aggregated structure of primary nanosized particles, while the particles prepared from an aqueous solution showed a dense structure of agglomerated primary particles.

Other methods to prepare nanocrystalline CeO_2-based powders are hydrothermal synthesis [109-113], solid state reaction at room temperature [114], freeze-drying [115], chemical vapor deposition [116], flame spray pyrolysis [117], sonochemical [118], sol-gel [95] and gas condensation [119].

Nanocrystalline particles with high surface area usually result in a stronger tendency for the powder to agglomerate which make processing difficult and the expected benefits of the small particles could be lost [95]. By precipitation [120] it is difficult to avoid growth and agglomeration of particles, but this could be inhibited by a combined method of homogenous precipitation with microemulsion with ammonium hydroxide [121], methyl oxalate [122] or aqueous sodium hydroxide [123]. To reduce the size of the soft agglomerates the common procedure is ball milling.

Among the reported powder synthesis techniques, precipitation is the most common route. Precipitation using carbonates are perhaps preferable due to lower degree of agglomeration which is an important parameter for further processing and densification. Commercial powders are available and relative inexpensive, but usually these powders show poorer densification properties.

$LaNbO_4$-based materials

Literature reveals little information about powder synthesis and densification of polycrystalline $LaNbO_4$-based materials. $LaNbO_4$ powders have mainly been prepared by solid state reaction method [10-13, 124], however this method generally gives powders with large particle size and large particle size distrubution. In addition, several repeated milling and calcination cycles increase the amount of impurities. Solution based methods are advantageous for the preparation of high quality powders with small particle size, but for materials with Nb(V) this is challenging due to the high valence of Nb(V) and thus fast hydrolysis of the niobium cation [125]. Hence, precursors for preparing aqueous niobium solutions are limited to Nb_2O_5 [126], $NbCl_5$ [127, 128], alkoxides of niobium [129, 130] and niobium ammonium oxalate [131, 132]. These precursors can be stabilized by complexing with e.g. tartaric acid [133-135], citric acid [132], DL-malic acid [128, 133, 136], hydrogen peroxide and citric acid [131, 137], making peroxo-carboxylato compounds [126] or by using the polymeric precursor method developed by Pechini [138]. Most of these precursors and some of the complexing agents are not suitable for large scale powder production due to e.g. toxicity and price.

Chemical methods using $NbCl_5$ and $LaCl_3$ have been used to prepare $LaNbO_4$ powders [139, 140] resulting in better sintering properties than powders prepared from solid state mixing of oxides. $LaNbO_4$, with an average particle size of ~1 μm, has also been prepared by co-precipitation of K_3NbO_4 and $LaCl_3$ [141].

3.3.2. Densification

Traditional sintering of materials based on CeO_2 or $LaNbO_4$ involves two steps: 1) Solid state mixing of different oxides, e.g. CeO_2 and Gd_2O_3 and La_2O_3 and Nb_2O_5, respectively, at high temperature (~1000°C) to obtain single phase powders and 2) Densification at even higher temperature,

typically >1500°C depending in composition. As mentioned above, a high quality powder is an important parameter to prepare materials with suitable properties. For densification, different sintering techniques are available. A literature review of different sintering techniques to prepare CeO_2 and $LaNbO_4$-based materials is presented in the following. For CeO_2, the review mainly addresses densification of nanocrystalline bulk materials.

CeO_2-based materials

Pressureless sintering of nanocrystalline powders are often accompanied by grain growth due to non-densifying processes, such as surface diffusion and evaporation-condensation, which are enhanced with an increase in surface area. Therefore the ceramics often looses their nanocrystalline character after densification. However, by using highly reactive nanocrystalline powders prepared by homogenous precipitation Li et al. [94] sintered Gd and Sm-substituted CeO_2 with grain size ~120 nm by pressureless sintering.

To decrease the sintering temperature, sintering promoters can be used, but these could increase the grain growth due to lower activation energy for grain growth compared to pure CeO_2. Adding CoO (< 1% atomic ratio) to CeO_2 [142] reduced the sintering temperature with approximately 200°C. The decrease in sintering temperature by adding CoO is also reported by others [60, 115, 143, 144]. CeO_2 added 1% MnO lowered the sintering temperature by more than 200°C and promoted grain boundary mobility [145]. The effect of manganese doping on sintering of commercial CeO_2 powders has been studied. Mn-doped CeO_2 increased the sintered density compared to pure CeO_2, but further doping (>5 at% Mn) did not affect the density [59]. Ga_2O_3 has also been introduced to commercial powders of $Ce_{0.8}Gd_{0.2}O_{1.9}$ to increase the density. A maximum in density was observed for 0.5 mol% Ga_2O_3 addition [146]. Fe_2O_3 added by mechanical mixing or wet chemical route to $Ce_{0.9}Gd_{0.1}O_{2-\delta}$ reduced the temperature for maximum sintering, but the effect on grain size was small [56, 147].

Fully dense CeO_{2-x} and Gd-substituted CeO_2 polycrystals of ~10 nm has been prepared by hot pressing at a unusually high pressure of 1.1 GPa at 600°C and this is the lowest grain size achieved in dense polycrystalline CeO_2-based materials [36, 37]. Hot pressing at 645°C at 700 MPa resulted in 92% dense samples grain size of 26 nm determined from X-ray diffraction profiles [148].

Spark plasma sintering (SPS) is a relatively new sintering technique to consolidate powders of various oxides and non-oxides [149]. The technique is similar to hot pressing where a uniaxial pressure is applied during sintering. The main difference is the heating source. A pulsed direct current is applied and allowed to pass through an electrically conducting die and therefore through the sample. Because of the efficient thermal transfer, the applied pressure (< 140 MPa [150]) and the presence of an electrical field that most possibly enhances diffusion/grain growth process, very fast densification can be achieved. It has been shown [149] that the conversion from nano to microsized grains is very temperature dependent and above a critical temperature (T_g) grain growth occurs very rapidly. Below T_g nano-grained structures are stable against grain growth. There are few reported studies of preparation of CeO_2-based materials by SPS. The reason for this is that carbon has been observed to penetrate from the graphite die into the specimen, preventing the densification of the sample [51]. But recently, dense CeO_2-based bulk materials with grain size of 15 nm were prepared at ~700°C for 5 min by SPS using a modified die allowing an unusually high pressure of 1 GPa [150]. Mori et al. [51] prepared dense $Ce_{0.8}Dy_{0.2}O_{1.9}$ by a combination of SPS and conventional sintering resulting in higher conductivity and lower activation energy compared to samples prepared by conventional sintering due to smaller microdomains. The average grain size was approximately similar between the two densification techniques.

Other densification techniques, which have not been applied for CeO_2-based materials, are e.g. two step sintering and sinter-forging. Chen et al. prepared fully dense bulk materials of Y_2O_3 with grain size of 60 nm by two step sintering method without applied pressure. The samples was first heated rapidly to achieve intermediate density (> 75%) and then cooled to a lower temperature for further densification. The materials exhibit pores unstable against shrinkage after the first step and these pores can be filled as long as the grain boundary diffusion allows it, even if the particle network is frozen as it is in the second step [151]. Agglomerated powders might cause green bodies with large pores which are difficult to remove by pressureless sintering. Sinter-forging, a die-less compression of a powder, could effectively remove these large pores and result in high density with small grains, as demonstrated for e.g. zirconia [152].

Independent of which sintering technique used the grain size is usually influenced by partly substitution of other cations. Hwang and Chen [153] demonstrated that di- and trivalent cations substituted in Y-TZP inhibited grain growth, while tetra- and pentavalent cations did not affect the grain size. The reason for the reduced grain growth is segregation of lower valent cations to the positively charged grain boundary, due to oxygen vacancies

lowering the grain boundary mobility. Similar observations are usually observed in CeO_2-based materials [91, 110, 154]. Adding cations with larger radii (e.g. Ca^{2+}, Y^{3+} and Nd^{3+}) compared to Ce^{4+} resulted in smaller grains, while adding smaller cations (e.g. Mg^{2+} and Sc^{3+}) increased the grain size and lowered the final density [110]. In the latter work, the maximum densification rate was shifted to higher temperatures in the substituted materials due to reduced rate of grain boundary diffusion. The lower final density might be due to that the powders with Mg^{2+} and Sc^{3+} had a bimodal particle size distribution.

A reduction in sintering temperature is not only important concerning the grain size, but also to achieve high density. As CeO_2-based materials are reduced during sintering at high temperatures [102, 155, 156], see Chapter 3.2.1., and the gaseous species formed causes porosity, decreasing the density. The degree of reduction has been reported to be more severe during high temperatures sintering using nanocrystalline compared to microcrystalline powders [155].

Commercially pure, nanocrystalline powders added sintering aids reducing the sintering temperature and thus the grain size has become a more interesting route since there lately has been observed an increase in grain boundary conductivity due to a scavenging effect of SiO_2 by adding Fe_2O_3 as sintering aid. Densification of nanocrystalline CeO_2-based bulk materials with very small grains (< 30 nm) has been achieved, but only by applying very high pressures during either hot pressing or spark plasma sintering. These methods are scarcely economical and commercially and more research on pressureless sintering of highly reactive powders are important.

$LaNbO_4$-based materials

Usually, polycrystalline $LaNbO_4$ materials are sintered in the temperature range of 1400-1600°C [11, 157, 158]. However, $LaNbO_4$ from wet chemical methods have been sintered at lower temperatures. Jian et al. [139] prepared 94% dense $LaNbO_4$ at 1270°C from powder prepared by chemical method. Maschio et al. [159] prepared powder by coprecipitation and dilatometer studies revealed a wide temperature window (1000-1450°C) for densification. Takagi et al. [160] prepared dense $LaNbO_4$ and $LaNbO_4/Al_2O_3$ composites by spark plasma sintering at 1300°C for 5 min while applying a pressure of 30 MPa. Pure $LaNbO_4$ ceramics had an average grain size of 18 μm. Due to the recently reported proton conductivity in LaNbO4-based materials further investigation of powder synthesis and densification are of importance.

3.4. Mechanical properties

CeO_2-based materials

Ceramics that are promising candidates as solid electrolytes due to high ionic conductivity and chemical stability in operating conditions must also have suitable mechanical properties. Compared to materials based on zirconia, CeO_2-based materials have poorer mechanical properties. In addition, the larger cell volume in reduced CeO_2 compared to stoichiometric CeO_2 and partial reduction due to exposure of different $p(O_2)$ induces stress in the material. This chemical induced stress will be deleterious to the mechanical properties of the electrolyte [161], but can be inhibited by coating the fuel side of the electrolyte with a thin layer of YSZ as described earlier or lowering the operation temperature below 750°C [162].

In Table 1 hardness and fracture toughness are summarized for pure and Sm- and Gd-substituted CeO_2 materials reported in literature. In addition, values for 8YSZ are shown for comparison. The hardness and fracture toughness were strongly dependent on preparation techniques. The values for hardness and fracture toughness of 8YSZ ranged from 9.2 to 18.1 GPa and 2.4 to 3.1 $MPa \cdot m^{1/2}$, respectively [163]. There is a wide scattering in the values, especially regarding the fracture toughness, which is partly due to different measuring methods. Thus, the influence of composition on fracture toughness is not possible to determine. Pure CeO_2 show lower hardness (~4 GPa) compared to the substituted CeO_2-based materials (7-9 GPa).

The fracture toughness and hardness of $Ce_{0.8}Gd_{0.2}O_{2-\delta}$ could be increased by adding Al_2O_3. An increase in fracture toughness, from 1.5 up to 2.6 $MPa \cdot m^{1/2}$, and hardness, from 9.2 GPa up to 10.5 GPa, by increased amount of Al_2O_3 up to 20% in $Ce_{0.8}Gd_{0.2}O_{2-\delta}$ has been demonstrated [58]. But, as mentioned earlier, addition of Al_2O_3 reduces the ionic conductivity of the materials. Zhang et al. [164] prepared $Ce_{0.8}Gd_{0.2}O_{2-\delta}$ with different grain sizes (0.53 - 9.50 μm) and found no dependence between grain size and fracture toughness. A slight increase in hardness with grain size was observed in the same work.

Table 1 Literature values of hardness and fracture toughness for CeO_2-based materials.

Composition	Density (%)	Hardness (GPa)	Fracture toughness ($MPa \cdot m^{1/2}$)	Testing method [1]	Ref
CeO_2	94	~3.9	~1.4	SENB	[165]
$Ce_{0.8}Gd_{0.2}O_{2-\delta}$	>97	9.2±0.4	1.47±0.20	Indentation	[58]
$Ce_{0.8}Gd_{0.2}O_{2-\delta}$	99		1.05	Indentation	[166]
$Ce_{0.8}Gd_{0.2}O_{2-\delta}$	95		2.08±0.31	Indentation	[167]
$Ce_{0.8}Gd_{0.2}O_{2-\delta}$	>99	9.3±0.1 [2]	1.53±0.20	Indentation	[164]
$Ce_{0.8}Sm_{0.2}O_{2-\delta}$	99		0.90	Indentation	[166]
$Ce_{0.8}Sm_{0.2}O_{2-\delta}$	94	8.6±0.25	2.4±0.3	Indentation	[168]
$Ce_{0.8}Sm_{0.2}O_{2-\delta}$	94	8.6±0.25	1.35±0.15	SENB	[168]
$Ce_{0.8}Sm_{0.2}O_{1.9}$	98	7.2±1.3			[169]
$Ce_{0.9}Sm_{0.1}O_{2-\delta}$	96	8.7±0.25	2.4±0.3	Indentation	[168]
$Ce_{0.9}Sm_{0.1}O_{2-\delta}$	96	8.7±0.25	1.28±0.15	SENB	[168]
8YSZ	96	9.2-18.1	2.4-3.1	Indentation	[163]

[1] Values of fracture toughness by indentation for CeO_2-based materials are all calculated from equation (I-5) in Appendix I.
[2] Average value. Hardness increased from 8.25 GPa to 9.75 GPa by increased grain size (0.53 - 9.50 μm).

$LaNbO_4$-based materials

The mechanical properties of $LaNbO_4$-based materials are poorly studied. For pure $LaNbO_4$, only one paper is published where Takagi et al. [160] prepared $LaNbO_4$ by spark plasma sintering and measured a 3-point fracture strength of 35 MPa. The low fracture strength was probably due to weak grain boundaries due to large grain size and possible microcracking. Adding 5 or 10 vol% Al_2O_3 increased the fracture strength to 160 or 250 MPa, respectively. In addition, an increase in strength by adding $LaNbO_4$ to CeO_2-stabilized tetragonal zirconia (Ce-TZP) [159] and to Al_2O_3 [141] has been demonstrated.

$LaNbO_4$ is ferroelastic in the low temperature monoclinic phase [139, 170]. Ferroelastic behavior of $LaNbO_4$ has been evidenced by a non-linear stress-strain relationship and a permanent deformation (0.17%) after unloading [139]. According to Aizu [171] a crystal is said to be ferroelastic when it has two or more orientation states in the absence of mechanical stress which can be shifted from one to another of these states by exposure to a mechanical stress. During cooling from the tetragonal to the monoclinic phase the change in lattice parameters resulting in an increased lattice strain energy. To accommodate for the increased energy, domains are created. For

$LaNbO_4$ the domains are orientated in two different directions separated by a boundary, reported to be between (2 0 -4)/(4 0 2) [172] and (2 0 -5)/(5 0 2) [173]. An important characteristic of ferroelastic materials is the existence of a hysteresis loop between the strain, ε, and applied stress, σ, as illustrated in Figure 11. The remnant strain, ε_r, represents the macroscopic deformation of the sample without external stress after compression. The coercive stress, σ_c, is defined as the intersection of the elastic hysteresis with the stress axis [174].

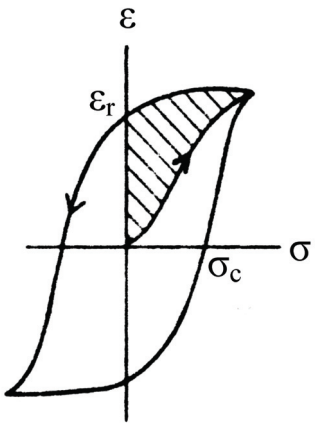

Figure 11 Schematic illustration of hysteresis loop for ferroelastic material, redrawn from Virkar [175]. ε_r is the remnant strain, σ_c is the coercive stress and the shaded area is the energy absorbed during domain reorientation.

Ferroelasticity is proposed to increase the fracture toughness due to absorption of mechanical energy related to the domain reorientation. When domains are reoriented, more energy is necessary for further crack propagation resulting in increased fracture toughness. Increased fracture toughness due to ferroelasticity have been reported for $LaFeO_3$ [176], $LaCoO_3$ [177] and t-ZrO_2 [175].

4. REFERENCES

[1] B. C. H. Steele and A. Heinzel, "*Materials for fuel-cell technologies*", Nature, 414 [6861] (2001) 345-352.

[2] N. Q. Minh, "*Ceramic fuel-cells*", J. Am. Ceram. Soc., 76 [3] (1993) 563-588.

[3] A. Hammou and J. Guindet, *Solid Oxide Fuel Cells*, in The CRC Handbook of Solid State Electrochemistry. (H. J. M. Bouwmeester and P. J. Gellings, eds.), CRC Press, Boxa Raton, (2000) 407-442.

[4] T. Norby, R. Haugsrud and N. Vajeeston, "*New Proton Conducting Materials for Fuel Cells and Hydrogen Separation Membranes*", Proc. 9th Int. Conf. on Inorganic Membranes, Lillehammer - Norway, (2006) 260-267.

[5] H. Matzke, *Diffusion in Nonstoichiometric Oxides*, in Nonstoichiometric Oxides. (O. T. Sørensen, ed.), Academic Press Inc., London, (1981) 155-232.

[6] M. Mogensen, N. M. Sammes and G. A. Tompsett, "*Physical, chemical and electrochemical properties of pure and doped ceria*", Solid State Ionics, 129 [1-4] (2000) 63-94.

[7] B. Zachau-Christiansen, T. Jacobsen and S. Skaarup, "*Electrochemical determination of oxygen stoichiometry and entropy in oxides*", Solid State Ionics, 86-8 (1996) 725-731.

[8] S. Tsunekawa, T. Kamiyama, K. Sasaki, H. Asano and T. Fukuda, "*Precise structure-analysis by neutron-diffraction for $RNbO_4$ and distortion of NbO_4 tetrahedra*", Acta Crystallogr. A, 49 (1993) 595-600.

[9] W. I. F. David, "*The high-temperature paraelastic structure of $LaNbO_4$*", Mat. Res. Bull., 18 [6] (1983) 749-756.

[10] L. Jian and C. M. Wayman, "*Monoclinic-to-tetragonal phase transformation in a ceramic rare-earth orthoniobate, $LaNbO_4$*", J. Am. Ceram. Soc., 80 [3] (1997) 803-806.

[11] V. S. Stubican, "*High-temperature transitions in rare-earth niobates and tantalates*", J. Am. Ceram. Soc., 47 [2] (1964) 55-58.

[12] H. Takei and S. Tsunekawa, "*Growth and properties of $LaNbO_4$ and $NdNbO_4$ single-crystals*", J. Cryst. Growth, 38 [1] (1977) 55-60.

[13] L. H. Brixner, J. F. Whitney, F. C. Zumsteg and G. A. Jones, "*Ferroelasticity in $LnNbO_4$-type rare-earth niobates*", Mat. Res. Bull., 12 [1] (1977) 17-24.

[14] B. C. H. Steele, *Oxygen ion conductors*, in High Conductivity Solid Ionic Conductors, Recent Trends and Applications. (T. Takahashi, ed.), World Scientific, Singapore, (1989) 402-446.

[15] H. Inaba and H. Tagawa, "*Ceria-based solid electrolytes - Review*", Solid State Ionics, 83 [1-2] (1996) 1-16.

[16] R. J. Panlener, R. N. Blumenthal and J. E. Garnier, "*Thermodynamic study of nonstoichiometric cerium dioxide*", J. Phys. Chem. Solids, 36 [11] (1975) 1213-1222.

[17] H. L. Tuller and A. S. Nowick, "*Small polaron electron-transport in reduced CeO_2 single-crystals*", J. Phys. Chem. Solids, 38 [8] (1977) 859-867.

[18] R. N. Blumenthal, P. W. Lee and R. J. Panlener, "*Studies of defect structure of nonstoichiometric cerium dioxide*", J. Electrochem. Soc., 118 [1] (1971) 123-129.

[19] J. A. Kilner, "*Fast oxygen transport in acceptor doped oxides*", Solid State Ionics, 129 [1-4] (2000) 13-23.

[20] K. Eguchi, T. Setoguchi, T. Inoue and H. Arai, "*Electrical-properties of ceria-based oxides and their application to solid oxide fuel-cells*", Solid State Ionics, 52 [1-3] (1992) 165-172.

[21] H. Yahiro, K. Eguchi and H. Arai, "*Electrical-properties and reducibilities of ceria rare earth oxide systems and their application to solid oxide fuel-cell*", Solid State Ionics, 36 [1-2] (1989) 71-75.

[22] B. C. H. Steele, "*Appraisal of $Ce_{1-y}Gd_yO_{2-y/2}$ electrolytes for IT-SOFC operation at 500°C*", Solid State Ionics, 129 [1-4] (2000) 95-110.

[23] T. Kobayashi, S. R. Wang, M. Dokiya, H. Tagawa and T. Hashimoto, "*Oxygen nonstoichiometry of $Ce_{1-y}Sm_yO_{2-0.5y-x}$ (y = 0.1, 0.2)*", Solid State Ionics, 126 [3-4] (1999) 349-357.

[24] S. R. Wang, H. Inaba, H. Tagawa, M. Dokiya and T. Hashimoto, "*Nonstoichiometry of $Ce_{0.9}Gd_{0.1}O_{1.95-x}$*", Solid State Ionics, 107 [1-2] (1998) 73-79.

[25] S. Wang, H. Inaba, H. Tagawa and T. Hashimoto, "*Nonstoichiometry of $Ce_{0.8}Gd_{0.2}O_{1.9-x}$*", J. Electrochem. Soc., 144 [11] (1997) 4076-4080.

[26] D. Schneider, M. Godickemeier and L. J. Gauckler, "*Nonstoichiometry and defect chemistry of ceria solid solutions*", J. Electroceram., 1 [2] (1997) 165-172.

[27] T. Inoue, T. Setoguchi, K. Eguchi and H. Arai, "*Study of a solid oxide fuel-cell with a ceria-based solid electrolyte*", Solid State Ionics, 35 [3-4] (1989) 285-291.

[28] A. Atkinson and A. Selcuk, "*Mechanical behaviour of ceramic oxygen ion-conducting membranes*", Solid State Ionics, 134 [1-2] (2000) 59-66.

[29] X. D. Zhou, B. Scarfino and H. U. Anderson, "*Electrical conductivity and stability of Gd-doped ceria/Y-doped zirconia ceramics and thin films*", Solid State Ionics, 175 [1-4] (2004) 19-22.

[30] H. L. Tuller, "*Ionic conduction in nanocrystalline materials*", Solid State Ionics, 131 [1-2] (2000) 143-157.

[31] C. Y. Tian and S. W. Chan, "*Ionic conductivities, sintering temperatures and microstructures of bulk ceramic CeO_2 doped with Y_2O_3*", Solid State Ionics, 134 [1-2] (2000) 89-102.

[32] R. Gerhardt and A. S. Nowick, "*Grain-boundary effect in ceria doped with trivalent cations. 1. Electrical measurements*", J. Am. Ceram. Soc., 69 [9] (1986) 641-646.

[33] D. Y. Wang and A. S. Nowick, "*The grain-boundary effect in doped ceria solid electrolytes*", J. Solid State Chem., 35 [3] (1980) 325-333.
[34] J. Maier, "*Ionic-conduction in-space charge regions*", Prog. Sol. State Chem., 23 [3] (1995) 171-263.
[35] T. Suzuki, I. Kosacki, H. U. Anderson and P. Colomban, "*Electrical conductivity and lattice defects in nanocrystalline cerium oxide thin films*", J. Am. Ceram. Soc., 84 [9] (2001) 2007-2014.
[36] Y. M. Chiang, E. B. Lavik and D. A. Blom, "*Defect thermodynamics and electrical properties of nanocrystalline oxides: Pure and doped CeO_2*", Nanostruct. Mater., 9 [1-8] (1997) 633-642.
[37] Y. M. Chiang, E. B. Lavik, I. Kosacki, H. L. Tuller and J. Y. Ying, "*Defect and transport properties of nanocrystalline CeO_{2-x}*", Appl. Phys. Lett., 69 [2] (1996) 185-187.
[38] A. Tschöpe, S. Kilassonia, B. Zapp and R. Birringer, "*Grain-size-dependent thermopower of polycrystalline cerium oxide*", Solid State Ionics, 149 [3-4] (2002) 261-273.
[39] S. Tsunekawa, R. Sivamohan, S. Ito, A. Kasuya and T. Fukuda, "*Structural study on monosize CeO_{2-x} nano-particles*", Nanostruct. Mater., 11 [1] (1999) 141-147.
[40] A. Tschöpe and R. Birringer, "*Oxyreduction studies on nanostructured cerium oxide*", Nanostruct. Mater., 9 [1-8] (1997) 591-594.
[41] I. Kosacki, V. Petrovsky, H. U. Anderson and P. Colomban, "*Raman spectroscopy of nanocrystalline ceria and zirconia thin films*", J. Am. Ceram. Soc., 85 [11] (2002) 2646-2650.
[42] I. Kosacki, T. Suzuki, V. Petrovsky and H. U. Anderson, "*Electrical conductivity of nanocrystalline ceria and zirconia thin films*", Solid State Ionics, 136 (2000) 1225-1233.
[43] T. Suzuki, I. Kosacki and H. U. Anderson, "*Defect and mixed conductivity in nanocrystalline doped cerium oxide*", J. Am. Ceram. Soc., 85 [6] (2002) 1492-1498.
[44] G. M. Christie and F. P. F. van Berkel, "*Microstructure - Ionic conductivity relationships in ceria-gadolinia electrolytes*", Solid State Ionics, 83 [1-2] (1996) 17-27.
[45] X. D. Zhou, W. Huebner, I. Kosacki and H. U. Anderson, "*Microstructure and grain-boundary effect on electrical properties of gadolinium-doped ceria*", J. Am. Ceram. Soc., 85 [7] (2002) 1757-1762.
[46] Y. R. Wang, T. Mori, J. G. Li and J. Drennan, "*Synthesis, characterization, and electrical conduction of 10 mol% Dy_2O_3 doped CeO_2 ceramics*", J. Eur. Ceram. Soc., 25 [6] (2005) 949-956.
[47] X. Guo, W. Sigle and J. Maier, "*Blocking grain boundaries in yttria-doped and undoped ceria ceramics of high purity*", J. Am. Ceram. Soc., 86 [1] (2003) 77-87.
[48] T. Mori, J. Drennan, J. H. Lee, J. G. Li and T. Ikegami, "*Oxide ionic conductivity and microstructures of Sm- or La-doped CeO_2-based systems*", Solid State Ionics, 154 (2002) 461-466.

[49] F. Y. Wang, B. Z. Wan and S. F. Cheng, "*Study on Gd^{3+} and Sm^{3+} co-doped ceria-based electrolytes*", J. Solid State Electrochem., 9 [3] (2005) 168-173.

[50] T. Mori, Y. R. Wang, J. Drennan, G. Auchterlonie, J. G. Li and T. Ikegami, "*Influence of particle morphology on nanostructural feature and conducting property in Sm-doped CeO_2 sintered body*", Solid State Ionics, 175 [1-4] (2004) 641-649.

[51] T. Mori, T. Kobayashi, Y. Wang, J. Drennan, T. Nishimura, J. G. Li and H. Kobayashi, "*Synthesis and characterization of nano-hetero-structured Dy doped CeO_2 solid electrolytes using a combination of spark plasma sintering and conventional sintering*", J. Am. Ceram. Soc., 88 [7] (2005) 1981-1984.

[52] T. S. Zhang, J. Ma, H. Cheng and S. H. Chan, "*Ionic conductivity of high-purity Gd-doped ceria solid solutions*", Mat. Res. Bull., 41 [3] (2006) 563-568.

[53] T. S. Zhang, J. Ma, S. H. Chan, P. Hing and J. A. Kilner, "*Intermediate-temperature ionic conductivity of ceria-based solid solutions as a function of gadolinia and silica contents*", Solid State Sci., 6 [6] (2004) 565-572.

[54] T. S. Zhang, P. Hing, H. T. Huang and J. Kilner, "*Ionic conductivity in the CeO_2-Gd_2O_3 system ($0.05 \leq Gd/Ce \leq 0.4$) prepared by oxalate coprecipitation*", Solid State Ionics, 148 [3-4] (2002) 567-573.

[55] S. W. Zha, C. R. Xia and G. Y. Meng, "*Effect of Gd (Sm) doping on properties of ceria electrolyte for solid oxide fuel cells*", J. Power Sources, 115 [1] (2003) 44-48.

[56] T. S. Zhang, J. Ma, J. Chan and J. A. Kilner, "*Grain boundary conduction of $Ce_{0.9}Gd_{0.1}O_{2-\delta}$ ceramics derived from oxalate coprecipitation: effects of Fe loading and sintering temperature*", Solid State Ionics, 176 [3-4] (2005) 377-384.

[57] T. S. Zhang, J. Ma, L. B. Kong, S. H. Chan, P. Hing and J. A. Kilner, "*Iron oxide as an effective sintering aid and a grain boundary scavenger for ceria-based electrolytes*", Solid State Ionics, 167 [1-2] (2004) 203-207.

[58] T. S. Zhang, Z. Q. Zeng, H. T. Huang, P. Hing and J. Kilner, "*Effect of alumina addition on the electrical and mechanical properties of $Ce_{0.8}Gd_{0.2}O_{2-\delta}$ ceramics*", Mater. Lett., 57 [1] (2002) 124-129.

[59] G. J. Pereira, R. H. R. Castro, D. Z. de Florio, E. N. S. Muccillo and D. Gouvea, "*Densification and electrical conductivity of fast fired manganese-doped ceria ceramics*", Mater. Lett., 59 [10] (2005) 1195-1199.

[60] T. S. Zhang, J. Ma, L. B. Kong, P. Hing, Y. J. Leng, S. H. Chan and J. A. Kilner, "*Sinterability and ionic conductivity of coprecipitated $Ce_{0.8}Gd_{0.2}O_{2-\delta}$ powders treated via a high-energy ball-milling process*", J. Power Sources, 124 [1] (2003) 26-33.

[61] T. Norby, "*Solid-state protonic conductors: principles, properties, progress and prospects*", Solid State Ionics, 125 [1-4] (1999) 1-11.

[62] H. Iwahara, T. Esaka, H. Uchida and N. Maeda, "*Proton conduction in sintered oxides and its application to steam electrolysis for hydrogen-production*", Solid State Ionics, 3-4 (1981) 359-363.

[63] T. Norby and Y. Larring, "*Concentration and transport of protons in oxides*", Curr. Opin. Solid State Mater. Sci., 2 [5] (1997) 593-599.
[64] T. Kudo, *Survey of Types of Solid Electrolytes*, in The CRC Handbook of Solid State Electrochemistry. (H. J. M. Bouwmeester and P. J. Gellings, eds.), CRC Press, Boxa Raton, (2000) 195-221.
[65] R. Haugsrud and T. Norby, "*Proton conduction in rare-earth ortho-niobates and ortho-tantalates*", Nat. Mater., 5 [3] (2006) 193-196.
[66] R. Haugsrud and T. Norby, "*High-Temperature Proton Conductivity in Acceptor-doped $LaNbO_4$*", Solid State Ionics, 177 [13-14] (2006) 1129-1135.
[67] K. D. Kreuer, "*Proton-conducting oxides*", Annu. Rev. Mater. Res, 33 (2003) 333-359.
[68] K. C. Liang and A. S. Nowick, "*High-temperature protonic conduction in mixed perovskite ceramics*", Solid State Ionics, 61 [1-3] (1993) 77-81.
[69] K. C. Liang, Y. Du and A. S. Nowick, "*Fast high-temperature proton transport in nonstoichiometric mixed perovskites*", Solid State Ionics, 69 [2] (1994) 117-120.
[70] T. Norby, O. Dyrlie and P. Kofstad, "*Protonic conduction in acceptor-doped cubic rare-earth sesquioxides*", J. Am. Ceram. Soc., 75 [5] (1992) 1176-1181.
[71] T. Norby and N. Christiansen, "*Proton conduction in Ca-substituted and Sr-substituted $LaPO_4$*", Solid State Ionics, 77 (1995) 240-243.
[72] K. Amezawa, Y. Kitajima, Y. Tomii and N. Yamamoto, "*High-temperature protonic conduction in LaP_3O_9*", Electrochem. Solid-State Lett., 7 [12] (2004) A511-A514.
[73] R. Haugsrud and T. Norby, Personal communication (2006)
[74] R. Haugsrud, B. Ballesteros, M. Lira-Cantu and T. Norby, "*Ionic and electronic conductivity of 5% Ca-doped $GdNbO_4$*", J. Electrochem. Soc., 153 [8] (2006) J87-J90.
[75] N. Bonanos, "*Transport-properties and conduction mechanism in high-temperature protonic conductors*", Solid State Ionics, 53-56 (1992) 967-974.
[76] K. C. Patil, S. T. Aruna and T. Mimani, "*Combustion synthesis: an update*", Curr. Opin. Solid State Mater. Sci., 6 [6] (2002) 507-512.
[77] K. C. Patil, S. T. Aruna and S. Ekambaram, "*Combustion synthesis*", Curr. Opin. Solid State Mater. Sci., 2 [2] (1997) 158-165.
[78] T. Mokkelbost, I. Kaus, T. Grande and M. A. Einarsrud, "*Combustion synthesis and characterization of nanocrystalline CeO_2-based powders*", Chem. Mater., 16 [25] (2004) 5489-5494.
[79] H. S. Potdar, S. B. Deshpande, Y. B. Khollam, A. S. Deshpande and S. K. Date, "*Synthesis of nanosized $Ce_{0.75}Zr_{0.25}O_2$ porous powders via an autoignition: glycine nitrate process*", Mater. Lett., 57 [5-6] (2003) 1066-1071.
[80] R. D. Purohit, B. P. Sharma, K. T. Pillai and A. K. Tyagi, "*Ultrafine ceria powders via glycine-nitrate combustion*", Mat. Res. Bull., 36 [15] (2001) 2711-2721.

[81] M. F. Bianchetti, R. E. Juarez, D. G. Lamas, N. E. W. de Reca, L. Perez and E. Cabanillas, "*Synthesis of nanocrystalline CeO_2-Y_2O_3 powders by a nitrate-glycine gel-combustion process*", J. Mater. Res., 17 [9] (2002) 2185-2188.

[82] Y. Ji, J. Liu, T. M. He, L. G. Cong, J. X. Wang and W. H. Su, "*Single intermedium-temperature SOFC prepared by glycine-nitrate process*", J. Alloy. Compd., 353 [1-2] (2003) 257-262.

[83] R. R. Peng, C. R. Xia, Q. X. Fu, G. Y. Meng and D. K. Peng, "*Sintering and electrical properties of $(CeO_2)_{0.8}(Sm_2O_3)_{0.1}$ powders prepared by glycine-nitrate process*", Mater. Lett., 56 [6] (2002) 1043-1047.

[84] I. Mahata, G. Das, R. K. Mishra and B. P. Sharma, "*Combustion synthesis of gadolinia doped ceria powder*", J. Alloy. Compd., 391 [1-2] (2005) 129-135.

[85] S. T. Aruna and K. C. Patil, "*Combustion synthesis and properties of nanostructured ceria-zirconia solid solutions*", Nanostruct. Mater., 10 [6] (1998) 955-964.

[86] S. T. Aruna, S. Ghosh and K. C. Patil, "*Combustion synthesis and properties of $Ce_{1-x}Pr_xO_{2-\delta}$ red ceramic pigments*", Int. J. Inorg. Mater., 3 [4-5] (2001) 387-392.

[87] W. F. Chen, F. S. Li and J. Y. Yu, "*Combustion synthesis and characterization of nanocrystalline CeO_2-based powders via ethylene glycol-nitrate process*", Mater. Lett., 60 [1] (2006) 57-62.

[88] L. A. Chick, L. R. Pederson, G. D. Maupin, J. L. Bates, L. E. Thomas and G. J. Exarhos, "*Glycine nitrate combustion synthesis of oxide ceramic powders*", Mater. Lett., 10 [1-2] (1990) 6-12.

[89] I. S. Park, S. J. Kim, B. H. Lee and S. Park, "*Sintering and electrical properties of $(CeO_2)_{0.9}(Gd_2O_3)_{0.1}$ powders prepared by glycine-nitrate process for solid oxide fuel cell applications*", Jpn. J. Appl. Phys. Part 1, 36 [10] (1997) 6426-6431.

[90] P. Duran, F. Capel, D. Gutierrez, J. I. Tartaj and C. Moure, "*Cerium (IV) oxide synthesis and sinterable powders prepared by the polymeric organic complex solution method*", J. Eur. Ceram. Soc., 22 [9-10] (2002) 1711-1721.

[91] J. Markmann, A. Tschöpe and R. Birringer, "*Low temperature processing of dense nanocrystalline yttrium-doped cerium oxide ceramics*", Acta Mater., 50 [6] (2002) 1433-1440.

[92] P. L. Chen and I. W. Chen, "*Reactive cerium(IV) oxide powders by the homogeneous precipitation method*", J. Am. Ceram. Soc., 76 [6] (1993) 1577-1583.

[93] M. Kamruddin, P. K. Ajikumar, R. Nithya, A. K. Tyagi and B. Raj, "*Synthesis of nanocrystalline ceria by thermal decomposition and soft-chemistry methods*", Scripta Mater., 50 [4] (2004) 417-422.

[94] J. G. Li, Y. R. Wang, T. Ikegami, T. Mori and T. Ishigaki, "*Reactive 10 mol% RE_2O_3 (RE = Gd and Sm) doped CeO_2 nanopowders: Synthesis, characterization, and low-temperature sintering into dense ceramics*", Mater. Sci. Eng. B:, 121 [1-2] (2005) 54-59.

[95] B. Djuricic and S. Pickering, "*Nanostructured cerium oxide: Preparation and properties of weakly-agglomerated powders*", J. Eur. Ceram. Soc., 19 [11] (1999) 1925-1934.

[96] F. Zhang, S. P. Yang, H. M. Chen and X. B. Yu, "*Preparation of discrete nanosize ceria powder*", Ceram. Int., 30 [6] (2004) 997-1002.

[97] S. Nakane, T. Tachi, M. Yoshinaka, K. Hirota and O. Yamaguchi, "*Characterization and sintering of reactive cerium(IV) oxide powders prepared by the hydrazine method*", J. Am. Ceram. Soc., 80 [12] (1997) 3221-3224.

[98] K. Higashi, K. Sonoda, H. Ono, S. Sameshima and Y. Hirata, "*Synthesis and sintering of rare-earth-doped ceria powder by the oxalate coprecipitation method*", J. Mater. Res., 14 [3] (1999) 957-967.

[99] J. G. Li, T. Ikegami, Y. R. Wang and T. Mori, "*10-mol%-Gd_2O_3-doped CeO_2 solid solutions via carbonate coprecipitation: A comparative study*", J. Am. Ceram. Soc., 86 [6] (2003) 915-921.

[100] J. G. Li, T. Ikegami, T. Mori and T. Wada, "*Reactive $Ce_{0.8}RE_{0.2}O_{1.9}$ (RE = La, Nd, Sm, Gd, Dy, Y, Ho, Er, and Yb) powders via carbonate coprecipitation. 1. Synthesis and characterization*", Chem. Mater., 13 [9] (2001) 2913-2920.

[101] Y. R. Wang, T. Mori, J. G. Li and T. Ikegami, "*Low-temperature synthesis of praseodymium-doped ceria nanopowders*", J. Am. Ceram. Soc., 85 [12] (2002) 3105-3107.

[102] H. B. Li, C. R. Xia, M. H. Zhu, Z. X. Zhou and G. Y. Meng, "*Reactive $Ce_{0.8}Sm_{0.2}O_{1.9}$ powder synthesized by carbonate coprecipitation: Sintering and electrical characteristics*", Acta Mater., 54 [3] (2006) 721-727.

[103] H. G. Li, T. Ikegami, Y. R. Wang and T. Mori, "*Reactive ceria nanopowders via carbonate precipitation*", J. Am. Ceram. Soc., 85 [9] (2002) 2376-2378.

[104] T. Tsuzuki and P. G. McCormick, "*Synthesis of ultrafine ceria powders by mechanochemical processing*", J. Am. Ceram. Soc., 84 [7] (2001) 1453-1458.

[105] Y. X. Li, X. Z. Zhou, Y. Wang and X. Z. You, "*Preparation of nano-sized CeO_2 by mechanochemical reaction of cerium carbonate with sodium hydroxide*", Mater. Lett., 58 [1-2] (2004) 245-249.

[106] S. Gopalan and S. C. Singhal, "*Mechanochemical synthesis of nano-sized CeO_2*", Scripta Mater., 42 [10] (2000) 993-996.

[107] Y. X. Li, W. F. Chen, X. Z. Zhou, Z. Y. Gu and C. M. Chen, "*Synthesis of CeO_2 nanoparticles by mechanochemical processing and the inhibiting action of NaCl on particle agglomeration*", Mater. Lett., 59 [1] (2005) 48-52.

[108] H. S. Kang, J. R. Sohn, Y. C. Kang, K. Y. Jung and S. B. Park, "*The characteristics of nano-sized Gd-doped CeO_2 particles prepared by spray pyrolysis*", J. Alloy. Compd., 398 [1-2] (2005) 240-244.

[109] C. Y. Wang, Y. T. Qian, Y. Xie, C. S. Wang, L. Yang and G. W. Zhao, "*A novel method to prepare nanocrystalline (7 nm) ceria*", Mater. Sci. Eng. B:, 39 [3] (1996) 160-162.

[110] M. N. Rahaman and Y. C. Zhou, "*Effect of solid-solution additives on the sintering of ultra-fine CeO_2 powders*", J. Eur. Ceram. Soc., 15 [10] (1995) 939-950.
[111] M. Hirano and E. Kato, "*Hydrothermal synthesis of nanocrystalline cerium(IV) oxide powders*", J. Am. Ceram. Soc., 82 [3] (1999) 786-788.
[112] H. S. Potdar, S. B. Deshpande, A. S. Deshpande, S. P. Gokhale, S. K. Date, Y. B. Khollam and A. J. Patil, "*Preparation of ceria-zirconia ($Ce_{0.75}Zr_{0.25}O_2$) powders by microwave-hydrothermal (MH) route*", Mater. Chem. Phys., 74 [3] (2002) 306-312.
[113] N. C. Wu, E. W. Shi, Y. Q. Zheng and W. J. Li, "*Effect of pH of medium on hydrothermal synthesis of nanocrystalline cerium(IV) oxide powders*", J. Am. Ceram. Soc., 85 [10] (2002) 2462-2468.
[114] X. H. Yu, F. Li, X. R. Ye, X. Q. Xin and Z. L. Xue, "*Synthesis of cerium(IV) oxide ultrafine particles by solid-state reactions*", J. Am. Ceram. Soc., 83 [4] (2000) 964-966.
[115] D. Perez-Coll, P. Nunez, J. R. Frade and J. C. C. Abrantes, "*Conductivity of CGO and CSO ceramics obtained from freeze-dried precursors*", Electrochim. Acta, 48 [11] (2003) 1551-1557.
[116] W. Bai, K. L. Choy, N. H. J. Stelzer and J. Schoonman, "*Thermophoresis-assisted vapour phase synthesis of CeO_2 and $Ce_xY_{1-x}O_{2-\delta}$ nanoparticles*", Solid State Ionics, 116 [3-4] (1999) 225-228.
[117] D. J. Seo, K. O. Ryu, S. B. Park, K. Y. Kim and R. H. Song, "*Synthesis and properties of $Ce_{1-x}Gd_xO_{2-x/2}$ solid solution prepared by flame spray pyrolysis*", Mat. Res. Bull., 41 [2] (2006) 359-366.
[118] L. X. Yin, Y. Q. Wang, G. S. Pang, Y. Koltypin and A. Gedanken, "*Sonochemical synthesis of cerium oxide nanoparticles - Effect of additives and quantum size effect*", J. Colloid Interface Sci., 246 [1] (2002) 78-84.
[119] N. Guillou, L. C. Nistor, H. Fuess and H. Hahn, "*Microstructural studies of nanocrystalline CeO_2 produced by gas condensation*", Nanostruct. Mater., 8 [5] (1997) 545-557.
[120] J. G. Li, T. Ikegami, J. H. Lee and T. Mori, "*Characterization and sintering of nanocrystalline CeO_2 powders synthesized by a mimic alkoxide method*", Acta Mater., 49 [3] (2001) 419-426.
[121] T. Masui, K. Fujiwara, K. Machida, G. Adachi, T. Sakata and H. Mori, "*Characterization of Cerium(IV) oxide ultrafine particles prepared using reversed micelles*", Chem. Mater., 9 [10] (1997) 2197-2204.
[122] Y. J. He, B. L. Yang and C. X. Cheng, "*Controlled synthesis of CeO_2 nanoparticles from the coupling route of homogenous precipitation with microemulsion*", Mater. Lett., 57 [13-14] (2003) 1880-1884.
[123] J. S. Lee, J. S. Lee and S. C. Choi, "*Synthesis of nano-sized ceria powders by two-emulsion method using sodium hydroxide*", Mater. Lett., 59 [2-3] (2005) 395-398.
[124] M. G. Zuev, "*Phase behavior of in the systems La_2O_3-B_2O_3-Ta_2O_5 and La_2O_3-B_2O_3-Nb_2O_5 in the subsolidus region*", Z. Neorg. Khim., 43 [7] (1998) 1229-1232.
[125] J. Livage, M. Henry and C. Sanchez, "*Sol-gel chemistry of transition-metal oxides*", Prog. Sol. State Chem., 18 [4] (1988) 259-341.

[126] D. Bayot, B. Tinant and M. Devillers, "*Water-soluble niobium peroxo complexes as precursors for the preparation of Nb-based oxide catalysts*", Catal. Today, 78 [1-4] (2003) 439-447.

[127] K. Ruth, R. Kieffer and R. Burch, "*Mo-V-Nb oxide catalysts for the partial oxidation of ethane - I. Preparation and structural characterisation*", J. Catal., 175 [1] (1998) 16-26.

[128] E. R. Camargo and M. Kakihana, "*Chemical synthesis of lithium niobate powders ($LiNbO_3$) prepared from water-soluble (DL)-malic acid complexes*", Chem. Mater., 13 [5] (2001) 1905-1909.

[129] J. H. Yi, P. Thomas, M. Manier, J. P. Mercurio, I. Jauberteau and R. Guinebretiere, "*$SrBi_2Nb_2O_9$ ferroelectric powders and thin films prepared by sol-gel*", J. Sol-Gel Sci. Technol., 13 [1-3] (1998) 885-888.

[130] W. Sakamoto, T. Yogo, K. Kikuta, K. J. Ogiso, A. Kawase and S. Hirano, "*Synthesis of strontium barium niobate thin films through metal alkoxide*", J. Am. Ceram. Soc., 79 [9] (1996) 2283-2288.

[131] Y. Narendar and G. L. Messing, "*Synthesis, decomposition and crystallization characteristics of peroxo-citrato-niobium: An aqueous niobium precursor*", Chem. Mater., 9 [2] (1997) 580-587.

[132] T. Asai, E. R. Camargo, M. Kakihana and M. Osada, "*A novel aqueous solution route to the low-temperature synthesis of $SrBi_2Nb_2O_9$ by use of water-soluble Bi and Nb complexes*", J. Alloy. Compd., 309 [1-2] (2000) 113-117.

[133] E. Ruzdic and N. Brnicevic, "*Coordination properties of alpha-hydroxy carboxylic-acids. 1.Binuclear niobium(V) complex acids and some salts*", Inorg. Chim. Acta, 88 [1] (1984) 99-103.

[134] J. C. Ray, A. B. Panda, C. R. Saha and P. Pramanik, "*Synthesis of niobium(V)-stabilized tetragonal zirconia nanocrystalline powders*", J. Am. Ceram. Soc., 86 [3] (2003) 514-516.

[135] R. N. Das and P. Pramanik, "*Chemical synthesis of fine powder of lead magnesium niobate using niobium tartarate complex*", Mater. Lett., 46 [1] (2000) 7-14.

[136] E. R. Camargo and M. Kakihana, "*Low temperature synthesis of lithium niobate powders based on water-soluble niobium malato complexes*", Solid State Ionics, 151 [1-4] (2002) 413-418.

[137] K. Van Werde, G. Vanhoyland, D. Nelis, D. Mondelaers, M. K. Van Bael, J. Mullens and L. C. Van Poucke, "*Phase formation of ferroelectric perovskite 0.75 $Pb(Zn_{1/3},Nb_{2/3})O_3$ - 0.25 $BaTiO_3$ prepared by aqueous solution-gel chemistry*", J. Mater. Chem., 11 [4] (2001) 1192-1197.

[138] S. M. Zanetti, E. B. Araujo, E. R. Leite, E. Longo and J. A. Varela, "*Structural and electrical properties of $SrBi_2Nb_2O_9$ thin films prepared by chemical aqueous solution at low temperature*", Mater. Lett., 40 [1] (1999) 33-38.

[139] L. Jian and C. M. Wayman, "*Compressive behavior and domain-related shape memory effect in $LaNbO_4$ ceramics*", Mater. Lett., 26 [1-2] (1996) 1-7.

[140] S. Maschio, A. Bachiorrini, R. Dimonte and L. Montanaro, "*Preparation and characterization of $LaNbO_4$ from amorphous precursors*", J. Mater. Sci., 30 [21] (1995) 5433-5437.
[141] Z. L. Zhang, L. Zhou, Y. G. Hu and L. Jiang, "*Preparation and characterization of Al_2O_3-$LaNbO_4$ composites*", Scripta Mater., 47 [9] (2002) 637-641.
[142] T. S. Zhang, P. Hing, H. T. Huang and J. Kilner, "*Sintering and grain growth of CoO-doped CeO_2 ceramics*", J. Eur. Ceram. Soc., 22 [1] (2002) 27-34.
[143] T. S. Zhang and J. Ma, "*Dense submicron-grained $Ce_{0.8}Gd_{0.2}O_{2-\delta}$ ceramics for SOFC applications*", Scripta Mater., 50 [8] (2004) 1127-1130.
[144] C. Kleinlogel and L. J. Gauckler, "*Sintering and properties of nanosized ceria solid solutions*", Solid State Ionics, 135 [1-4] (2000) 567-573.
[145] Z. Tianshu, P. Hing, H. Huang and J. Kilner, "*Sintering and densification behavior of Mn-doped CeO_2*", Mater. Sci. Eng. B:, 83 [1-3] (2001) 235-241.
[146] J. S. Lee, K. H. Choi, B. K. Ryu, B. C. Shin and I. S. Kim, "*Effects of gallia additions on sintering behavior of $Ce_{0.8}Gd_{0.2}O_{1.9}$ ceramics prepared by commercial powders*", J. Mater. Sci., 40 [5] (2005) 1153-1158.
[147] T. S. Zhang, J. Ma, Y. J. Leng and Z. M. He, "*Sintering, microstructure and grain growth of Fe-doped $Ce_{0.9}Gd_{0.1}O_{2-\delta}$ ceramics derived from oxalate coprecipitation*", J. Cryst. Growth, 274 [3-4] (2005) 603-611.
[148] A. Tschöpe, E. Sommer and R. Birringer, "*Grain size-dependent electrical conductivity of polycrystalline cerium oxide I. Experiments*", Solid State Ionics, 139 [3-4] (2001) 255-265.
[149] Z. J. Shen, H. Peng, J. Liu and M. Nygren, "*Conversion from nano- to micron-sized structures: experimental observations*", J. Eur. Ceram. Soc., 24 [12] (2004) 3447-3452.
[150] U. Anselmi-Tamburini, J. E. Garay and Z. A. Munir, "*Fast low-temperature consolidation of bulk nanometric ceramic materials*", Scripta Mater., 54 [5] (2006) 823-828.
[151] I. W. Chen and X. H. Wang, "*Sintering dense nanocrystalline ceramics without final-stage grain growth*", Nature, 404 [6774] (2000) 168-171.
[152] D. C. Hague and M. J. Mayo, "*Sinter-forging of nanocrystalline zirconia 1. Experimental*", J. Am. Ceram. Soc., 80 [1] (1997) 149-156.
[153] S. L. Hwang and I. W. Chen, "*Grain-size control of tetragonal zirconia polycrystals using the space-charge concept*", J. Am. Ceram. Soc., 73 [11] (1990) 3269-3277.
[154] D. D. Upadhyaya, R. Bhat, S. Ramanathan, S. K. Roy, H. Schubert and G. Petzow, "*Solute effect on grain-growth in ceria ceramics*", J. Eur. Ceram. Soc., 14 [4] (1994) 337-341.
[155] Y. C. Zhou and M. N. Rahaman, "*Effect of redox reaction on the sintering behavior of cerium oxide*", Acta Mater., 45 [9] (1997) 3635-3639.
[156] J. G. Li, T. Ikegami and T. Mori, "*Low temperature processing of dense samarium-doped CeO_2 ceramics: sintering and grain growth behaviors*", Acta Mater., 52 [8] (2004) 2221-2228.

[157] L. Jian, C. M. Huang, G. B. Xu and C. M. Wayman, "*The domain-structure of $LaNbO_4$ in the low-temperature monoclinic phase*", Mater. Lett., 21 [1] (1994) 105-110.

[158] H. P. Rooksby and E. A. D. White, "*Structures of 1-1 compounds of rare earth oxides with niobia and tantala*", Acta Crystallogr., 16 [9] (1963) 888-890.

[159] S. Maschio, G. Pezzotti and O. Sbaizero, "*Effect of $LaNbO_4$ addition on the mechanical properties of ceria-tetragonal zirconia polycrystal matrices*", J. Eur. Ceram. Soc., 18 [12] (1998) 1779-1785.

[160] T. Takagi, Y. -H. Choa, T. Sekino and K. Niihara, "*Fabrication and mechanical properties of $LaNbO_4$ and $LaNbO_4/Al_2O_3$*", Key Eng. Mater., 161-163 (1999) 181-184.

[161] A. Atkinson and T. M. G. M. Ramos, "*Chemically-induced stresses in ceramic oxygen ion-conducting membranes*", Solid State Ionics, 129 [1-4] (2000) 259-269.

[162] A. Atkinson, "*Chemically-induced stresses in gadolinium-doped ceria solid oxide fuel cell electrolytes*", Solid State Ionics, 95 [3-4] (1997) 249-258.

[163] I. Abraham and G. Gritzner, "*Powder preparation, mechanical and electrical properties of cubic zirconia ceramics*", J. Eur. Ceram. Soc., 16 [1] (1996) 71-77.

[164] T. S. Zhang, J. Ma, L. B. Kong, P. Hing and J. A. Kilner, "*Preparation and mechanical properties of dense $Ce_{0.8}Gd_{0.2}O_{2-\delta}$ ceramics*", Solid State Ionics, 167 [1-2] (2004) 191-196.

[165] S. Maschio, O. Sbaizero and S. Meriani, "*Mechanical properties in the ceria-zirconia system*", J. Eur. Ceram. Soc., 9 [2] (1992) 127-132.

[166] K. Sato, H. Yugami and T. Hashida, "*Effect of rare-earth oxides on fracture properties of ceria ceramics*", J. Mater. Sci., 39 [18] (2004) 5765-5770.

[167] N. Sammes, G. Tompsett, Y. J. Zhang, A. Cartner and R. Torrens, "*The structural and mechanical properties of $(CeO_2)_{1-x}(GdO_{1.5})_x$ electrolytes*", Denki Kagaku, 64 [6] (1996) 674-680.

[168] J. E. Shemilt, H. M. Williams, M. J. Edirisinghe, J. R. G. Evans and B. Ralph, "*Fracture toughness of doped-ceria ceramics*", Scripta Mater., 36 [8] (1997) 929-934.

[169] S. Sameshima, T. Ichikawa, M. Kawaminami and Y. Hirata, "*Thermal and mechanical properties of rare earth-doped ceria ceramics*", Mater. Chem. Phys., 61 [1] (1999) 31-35.

[170] S. Tsunekawa and H. Takei, "*Domain switching behavior of ferroelastic $LaNbO_4$ and $NdNbO_4$*", J. Phys. Soc. Japan, 40 [5] (1976) 1523-1524.

[171] K. Aizu, "*Possible species of ferroelastic crystals and of simultaneously ferroelectric and ferroelastic crystals*", J. Phys. Soc. Japan, 27 [2] (1969) 387-396.

[172] L. Jian and C. M. Wayman, "*Domain boundary and domain switching in a ceramic rare-earth orthoniobate $LaNbO_4$*", J. Am. Ceram. Soc., 79 [6] (1996) 1642-1648.

[173] O. Prytz and J. Tafto, "*Accurate determination of domain boundary orientation in $LaNbO_4$*", Acta Mater., 53 [2] (2005) 297-302.
[174] E. K. H. Salje, Phase Transitions in Ferroelastic and Co-Elastic Crystals. University Press, Cambridge, (1990)
[175] A. V. Virkar and R. L. K. Matsumoto, "*Ferroelastic domain switching as a toughening mechanism in tetragonal zirconia*", J. Am. Ceram. Soc., 69 [10] (1986) C224-C226.
[176] A. Fossdal, M. A. Einarsrud and T. Grande, "*Mechanical properties of $LaFeO_3$ ceramics*", J. Eur. Ceram. Soc., 25 [6] (2005) 927-933.
[177] K. Kleveland, N. Orlovskaya, T. Grande, A. M. M. Moe, M. A. Einarsrud, K. Breder and G. Gogotsi, "*Ferroelastic behavior of $LaCoO_3$-based ceramics*", J. Am. Ceram. Soc., 84 [9] (2001) 2029-2033.

Papers are not included due to copyright.